# Geological scatter of cosmogenic-nuclide exposure ages in the Shackleton Range, Antarctica: implications for glacial history

Quaternary Geochronology xxx (2013) 1–15

Contents lists available at SciVerse ScienceDirect

Quaternary Geochronology

journal homepage: www.elsevier.com/locate/quageo

Research paper

# Geological scatter of cosmogenic-nuclide exposure ages in the Shackleton Range, Antarctica: Implications for glacial history☆

Andrew S. Hein [a,*], Christopher J. Fogwill [b], David E. Sugden [a], Sheng Xu [c]

[a] School of GeoSciences, University of Edinburgh, Drummond Street, Edinburgh EH8 9XP, UK
[b] Climate Change Research Centre and School of Biological, Earth and Environmental Sciences, University of New South Wales, Sydney, NSW 2052, Australia
[c] Scottish Universities Environmental Research Centre, Rankine Avenue, East Kilbride G75 0QF, UK

ARTICLE INFO

*Article history:*
Received 19 March 2012
Received in revised form
21 November 2012
Accepted 15 March 2013
Available online xxx

*Keywords:*
Antarctic Ice Sheet
Cosmogenic nuclide surface exposure age dating
Geological scatter
Pleistocene
Quaternary
Beryllium
Aluminium
Last Glacial Maximum
Miocene

ABSTRACT

We use cosmogenic $^{26}Al/^{10}Be$ ratios in rocks from the Shackleton Range, Antarctica to investigate geological scatter, a challenge that faces exposure-age studies in Antarctica. Examining the scatter helps reveal the long-term lowering of Slessor Glacier, an outlet glacier of the East Antarctic Ice Sheet (EAIS) which flows into the Weddell Sea embayment. 144 $^{26}Al$ and $^{10}Be$ exposure ages from 72 samples are related to bedrock or clast sample characteristics and geomorphological measures of weathering, slope and stability. We explore this noisy dataset by using Principal Components Analysis (PCA) to identify patterns in the data. Despite noise, there exist correlations between age and degree of weathering and age and elevation above the adjacent ice surface. Clasts with young exposure ages have more complex exposure histories than those with old exposure ages. In terms of glacial history we show that (a) warm-based ice covered the upper slopes of the Shackleton Range millions of years ago and that the uplands have been mainly free of ice for more than 800 ka, (b) that Slessor Glacier's surface elevation was c. 150 m above present at c. 270 ka and c. 700 ka.



## 1. Introduction

Cosmogenic-nuclide exposure age dating has opened up new horizons into the glacial history of Antarctica (Balco, 2011). It has produced a body of field evidence dotted around the continent which makes it possible to identify the trajectory of change of the ice sheet over time scales of several centuries to millions of years. This deeper knowledge of the behaviour and longer-term trajectory of the ice sheet helps in assessing the significance of current geophysical measurements of change (Ivins and James, 2005; Whitehouse et al., 2012). In turn this helps refine glaciological models that are necessary to assess future ice-sheet change in a warming world.

Many exposure-age studies in Antarctica have revealed a wide scatter of ages (Ackert et al., 2007; Bentley et al., 2010; Bromley et al., 2010; Mackintosh et al., 2007; Stone et al., 2003; Storey et al., 2010; Todd et al., 2010). In many studies the aim has been to track thinning of the ice since the LGM as a means of improving the understanding of both ice-sheet behaviour and its effect on global sea-level change. Faced with what is termed "geological scatter" (cf. Balco, 2011), it is commonly assumed that the ice has emplaced some erratics with prior exposure – i.e. a boulder exposed for some time has been picked up by an overriding glacier and deposited elsewhere. On this basis anomalies may be identified, excluded from the analysis, and the interpretation of glacier thinning is based on the youngest clasts at any altitude (Bentley et al., 2010; Stone et al., 2003). In other cases it is argued that clasts accumulate on the ice surface in blue-ice ablation areas and have a scatter of ages before they are deposited (Ackert et al., 2011; Fogwill et al., 2012). In still other situations it can be shown that an exposed surface has been overridden by cold-based ice and survived the period of burial without disturbance, sometimes with deposition of occasional erratics (Briner et al., 2006; Sugden et al., 2005).



* Corresponding author. Tel.: 44 1316509140.
*E-mail address:* andy.hein@ed.ac.uk (A.S. Hein).

1871-1014/$ – see front matter © 2013 The Authors. Published by Elsevier B.V. All rights reserved.
http://dx.doi.org/10.1016/j.quageo.2013.03.008

There is also the issue of the subsequent weathering of a moraine. Hallet and Putkonen (1994) showed how erosion of a moraine leads to a scatter of ages younger than the age of the moraine. In a high-altitude part of the McMurdo Dry Valleys, Antarctica, Swanger et al. (2011) showed how clast size reduced from the glacier margin over a series of progressively older moraines which had been exposed for millions of years; the implication is that weathering breaks down the clasts and produces a scatter of younger ages mixed with the original older ages. In such cases the oldest exposure ages most closely date the moraine emplacement. There are also studies of ancient till surfaces in the high parts of the Dry Valleys, often with tundra polygons, which demonstrate that surfaces lower slowly through erosion and this leads to surface exposure ages that are younger than the original till deposit (Margerison et al., 2005; Morgan et al., 2011; Schafer et al., 1999). In some cases it is possible to determine the geomorphic process (e.g., moraine degradation or inheritance) that controls the exposure age distribution from a single moraine using statistical methods (Applegate et al., 2012).

This study of the Shackleton Range contributes to the debate about the significance of geological scatter in several ways. First, it comes from a new location in Antarctica. There are relatively few cosmogenic-nuclide studies from the Atlantic-facing Weddell Sea embayment. Second, the 72 samples related to one outlet glacier is one of the densest multi-nuclide datasets in Antarctica, and thus there is potential to unravel the multiple processes affecting geological scatter and learn the long-term glacial history. But there is one important cautionary note. The samples were selected in transects from the glacier margin to test a different hypothesis about thinning since the LGM. Thus we only sampled the freshest-looking, least-weathered samples at each location. To minimise the effects of the effect of weathering and disturbance we restricted our sampling to brick-sized clasts with long axes of 10–20 cm, preferably with glacial faceting indicating subglacial erosion (Hein et al., 2011). This sampling strategy means that our results will emphasize the youngest samples on the slopes.

The paper arises from the study of the elevation changes of the Slessor and Recovery glaciers, outlets of the East Antarctic Ice Sheet, during the Last Glacial Maximum (LGM) (Fig. 1). An initial paper suggested that the outlet glaciers had not thickened significantly during the LGM (Hein et al., 2011). Indeed only six out of 70 clasts revealed exposure ages younger than 50 ka, and these rocks were all on or at the glacier margin. The remaining 64 samples from the slopes overlooking Slessor Glacier display puzzling relationships and the $^{10}$Be surface exposure ages range from 110 ka to 1.6 Ma. There is no simple relationship between the scatter of ages and altitude above the glacier margin, suggesting that many different processes are at work both prior to clast deposition and afterwards. We explore such processes to gain an insight into the deeper glacial history of the mountains and the implications for exposure-age dating in Antarctic polar environments. This paper contributes 59 new $^{26}$Al exposure ages and 2 repeat $^{26}$Al/$^{10}$Be measurements to the original dataset, making a total of 144 $^{26}$Al and $^{10}$Be exposure ages from 72 rock samples (Hein et al., 2011).

## 2. Field area and approach

The Shackleton Range consists of basement rocks and in the context of the wider Transantarctic Mountains is unusual in that it is not capped by Beacon Supergroup sediments consisting mainly of sandstones (Kerr and Hermichen, 1999). The mountains boast a west-facing escarpment rising 700–800 m above the Filchner Ice

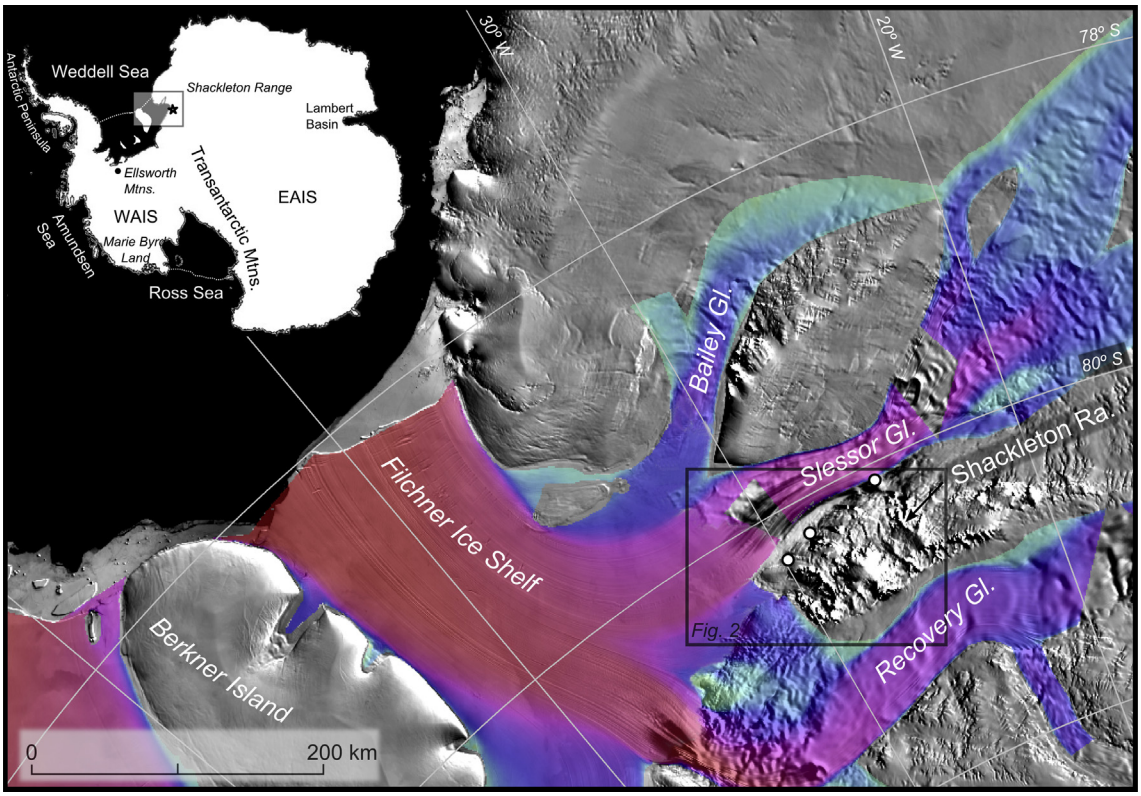


**Fig. 1.** The eastern Weddell Sea showing ice velocities for three major ice streams feeding the Filchner Ice Shelf; warm colours indicate fast flow-rates of up to 1500 m a$^{-1}$ (red), reducing to<100 m a$^{-1}$ (green) as illustrated by the progressively cooler colours (after Joughin and Bamber, 2005). The sample locations in the Shackleton Range are circled. After MODIS Mosaic of Antarctica image map (Haran et al., 2005) (figure adapted after Hein et al., 2011). (For interpretation of the references to colour in this figure legend, the reader is referred to the web version of this article.)

Please cite this article in press as: Hein, A.S., et al., Geological scatter of cosmogenic-nuclide exposure ages in the Shackleton Range, Antarctica: Implications for glacial history, Quaternary Geochronology (2013), http://dx.doi.org/10.1016/j.quageo.2013.03.008

Shelf which bounds a plateau which rises to ~1800 m before dipping gently beneath the East Antarctic Ice Sheet to the east (Höfle and Buggisch, 1995; Skidmore and Clarkson, 1972). Field observations of erosional landforms, striations and erratic lithologies show that the whole massif has been overridden by eroding ice at some stage in the past. Slessor Glacier to the north is 50 km wide and is overlooked on the Shackleton flank by gently rolling slopes studded with conical hills. Sporadic observations suggest that the cold, arid climate is similar to that of the McMurdo Dry Valleys, with occasional melting at low altitudes in summer but persistently sub-zero temperatures on the middle and upper slopes.

This study focuses on samples collected from the gentler slopes at three sites overlooking Slessor Glacier, namely, Mt. Provender which is moulded into the form of a large roche moutonnée, an area around Mt. Skidmore, and the flank of Mt. Sheffield (Fig. 2). The former two are bounded by local glaciers that grade into the surface of Slessor Glacier while the latter is situated on the margin of Slessor Glacier itself (Hein et al., 2011). To help investigate the observed complexity in the $^{10}$Be dataset we make detailed sample and site specific geomorphic observations to accompany each sample. Also we present new cosmogenic $^{26}$Al surface exposure ages for the same samples.

### 2.1. Geomorphic observations

Individual samples and field-sites were analysed through photographs and field observations. Within each site, samples are organised into groups defined by their geomorphic characteristics, namely altitude, slope angle and slope stability (Table 1). The latter measure varied from unstable till slopes with perched clasts and clear evidence of downslope movement of clasts, such as gelifluction lobes and talus creep, through intermediate measures such as the presence of upstanding stones adjacent to polygon boundaries indicating subsequent upthrusting, to apparently stable surfaces such as flat bedrock or till surfaces with few large or upstanding clasts and often 'ghost boulders' which have eroded away at the ground surface. Individual clasts were characterised in terms of lithology, size (length of long-axis), shape and degree of weathering. The latter measure was particularly useful in distinguishing between fresh rock surfaces, firm but iron-stained surfaces, and weathered clast surfaces with cracking, crumbling and/or weathering pits.

### 2.2. Interpreting the $^{26}$Al and $^{10}$Be data

Exposure histories can be investigated by comparing the concentration of two radionuclides with significantly different half lives. From the ratio it may be possible to detect whether the rock has experienced a complex exposure history such as periods of post-depositional burial beneath ice (Gosse and Phillips, 2001; Lal, 1991; Nishiizumi et al., 1989). This may be detected if the burial period is sufficiently long for significant decay of the short-lived isotope to occur.

In this study we measure the cosmogenic $^{26}$Al and $^{10}$Be concentrations and investigate the $^{26}$Al/$^{10}$Be ratios. The half-life of $^{26}$Al is about half that of $^{10}$Be and with continuous exposure the $^{26}$Al/$^{10}$Be ratio decreases as the isotopes decay, until their accumulation is matched by their loss through decay and the rock becomes saturated; the saturation point is reached sooner if the rock is also eroding. Thus, if a rock was continuously exposed and eroded at a continuous rate, its $^{26}$Al/$^{10}$Be ratio should plot within a well-defined zone dependent on the time of exposure and rate of erosion; this is termed a 'simple exposure' history (Fig. 3).

Complex exposure histories such as episodic erosion or prolonged periods of post-depositional burial can be detected if the $^{26}$Al/$^{10}$Be ratio plots below a line defining the erosion–saturation end points. In the case of burial, presumably by ice, the $^{26}$Al/$^{10}$Be ratio will lower due to faster decay of $^{26}$Al if the burial period is long enough. In the case of erosion, a ratio may plot in the complex zone if a large block fractures to expose a previously shielded surface. The new surface will have a similar $^{26}$Al/$^{10}$Be ratio but a lower concentration of $^{10}$Be and $^{26}$Al than the original surface due to attenuation of cosmic radiation with depth; this results in a leftward shift of the plotted $^{26}$Al/$^{10}$Be ratio (Fig. 3).

In the following discussion we make some assumptions on inheritance. In erosive conditions favoured by warm-based ice, we

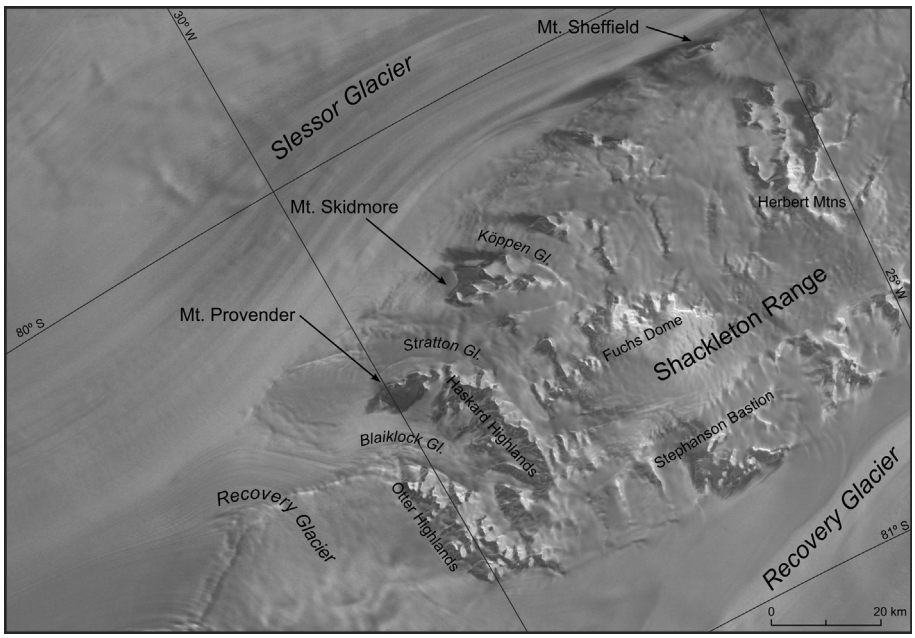


**Fig. 2.** A radar image of the Shackleton Range showing the three sites investigated and their relationship to local glaciers and the main shear zone of the Slessor Glacier. Image: RAMP AMM-1 SAR Image Mosaic of Antarctica (Jezek and Team, 2002).

Please cite this article in press as: Hein, A.S., et al., Geological scatter of cosmogenic-nuclide exposure ages in the Shackleton Range, Antarctica: Implications for glacial history, Quaternary Geochronology (2013), http://dx.doi.org/10.1016/j.quageo.2013.03.008

**Table 1**
Criteria for classifying geomorphic samples and groups. The scoring system is used for Principal Component Analysis.

| Sample | | | | | | | | Surface | | Results | |
|---|---|---|---|---|---|---|---|---|---|---|---|
| Lithology | | Shape | | Size (cm) | | Weathering | Elevation above ice | Slope | Stability | $^{10}$Be age (ka) | Exposure history |
| 1 | Conglomerate | 0 | Bedrock | 0 | Bedrock | 1 Very low degree of varnish | 1 0 – 100 m | 1 0–5° | 1 Bedrock | 1 0 – 100 | 0 No/high ratios |
| 2 | Schist | 1 | Angular | 1 | 1 – 10 | 2 Low to very low | 2 100 – 200 m | 2 5–10° | 2 Stable Till | 2 100 – 200 | 1 Simple |
| 3 | Sandstone | 2 | Sub-angular | 2 | 11 – 20 | 3 Low degree of varnish | 3 200 – 300 m | 3 10–20° | 3 Slightly modified till | 3 200 – 300 | 2 Complex |
| 4 | Volcanic | 3 | Sub-rounded | 3 | 21 – 30 | 4 Medium to low | 4 300 – 400 m | 4 >20° | 4 Modified till | 4 300 – 400 | |
| 5 | Granite | 4 | Rounded | 4 | 31 – 40 | 5 Medium degree of varnish | 5 400 – 500 m | | 5 Slightly active till | 5 400 – 500 | |
| 6 | Gneiss | | | 5 | 41 – 50 | 6 High to medium | 6 500 – 600 m | | 6 Active till | 6 500 – 600 | |
| 7 | Quartz | | | 6 | >50 | 7 High degree of varnish | 7 600 – 700 m | | 7 Highly active till | 7 600 – 700 | |
| 8 | Quartzite | | | | | | | | | 8 700 – 800 | |
| | | | | | | | | | | 9 800 – 900 | |
| | | | | | | | | | | 10 >900 | |

expect most clasts to have little or no inherited nuclides and thus, where these occur due to recycling and re-deposition of material, they should appear as a few outliers that are easily identifiable (e.g., Stone et al., 2003) or can be identified with statistical approaches (e.g., Porter and Swanson, 2008). Likewise, in a setting where the majority of clasts are recycled and re-deposited, we would expect inheritance in samples to show a random spread of exposure ages and a scatter of $^{26}$Al/$^{10}$Be ratios. In contrast, in a setting where inheritance developed in situ, for example, if the till survived burial beneath cold-based ice, we would expect a more organised cluster of values since they shared at least part of their exposure history.

In reality, the uncertainties in the $^{26}$Al and $^{10}$Be measurements and production rates make it difficult to distinguish samples with truly complex exposure histories from those with genuine simple exposures, and thus their interpretation relies on reasonable assumptions made from detailed geomorphic observations. In the following discussions we take the exposure history implied by the $^{26}$Al/$^{10}$Be ratio at face value. The term 'simple exposure' denotes samples with $^{26}$Al/$^{10}$Be ratios consistent with simple exposures within error margins. Likewise, since we compare different geomorphic 'groups' of $^{26}$Al/$^{10}$Be ratios collectively, we may refer to a population as showing more or less simple or complex exposure in order to highlight the direction of change.

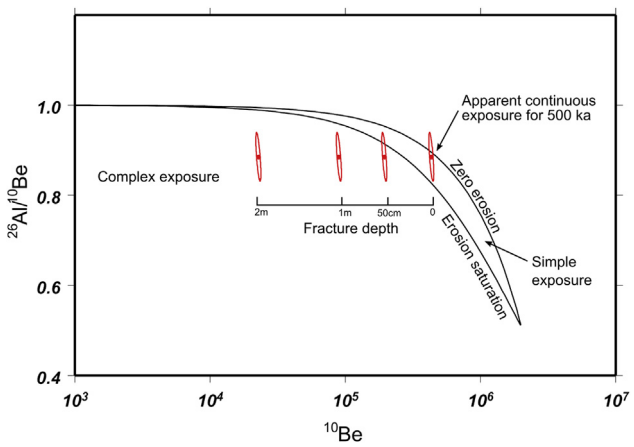


**Fig. 3.** Normalised plot of $^{26}$Al/$^{10}$Be vs $^{10}$Be concentration. Under continuous surface exposure and no erosion, the $^{26}$Al/$^{10}$Be ratio will follow the zero erosion line to saturation. If the surface is eroding, saturation will be reached sooner and the ratio will plot below the zero erosion line and above a line defined by the erosion saturation end points; this is termed a 'simple exposure history'. With prolonged post-depositional burial, the ratio will plot in the 'complex exposure' zone below the erosion saturation line (after Lal, 1991). The figure demonstrates how recent rock fracturing can affect the $^{26}$Al/$^{10}$Be ratio and introduce 'scatter' with a leftward shift of the ratio (Gosse and Phillips, 2001). Figure generated with the CRONUS-Earth exposure age calculator (Balco et al., 2008).

### 2.3. PCA

PCA is a statistical technique that explores the structure within multivariate datasets. It aims to take a large number of interrelated 'observed' variables (such as those listed in Table 1) and reduce the dimensionality of the dataset while preserving most of its variation. This is done by transforming the (possibly) correlated observed variables to a new set of (artificial) variables, the principal components, which are uncorrelated, and which are ordered such that the first few retain most of the variation present in all of the original observed variables (Jolliffe, 2002). In other words, it is useful for exploring data when the dominant variables are not known. For example, PCA helps to identify key correlations in a large dataset; much like a geomorphic map identifies key landforms within a complicated landscape. PCA does not allow for significance testing and thus the technique is best suited for hypothesis generation rather than testing (Kent and Coker, 1996). We apply PCA in this study because we are interested in exploring what correlations may or may not exist in the data without restriction to any particular dependent variable such as the exposure age. It is a useful starting point to identify underlying relationships in the data that can subsequently be refined and tested by more rigorous statistical methods such as multiple linear regression.

## 3. Results

Geomorphic maps of the three main sites of Mt. Provender, Mt. Skidmore and Mt. Sheffield and photographs show the surfaces typical for each sample group (Figs. 4–7). The location of each group is shown on the site maps. Table 1 describes the scoring system used for each variable while the individual sample scores are in Supplementary Table DR1. The cosmogenic nuclide data are presented in Tables 2 and 3. Details of the analyses, calculation method, scaling model and assumptions made are listed in the table footnotes. Further details, including additional photos and $^{26}$Al/$^{10}$Be ratio plots for each group are provided in the Supplementary Material.

### 3.1. Mt. Provender

Mt. Provender is located in the northwest of the range where the local Blaiklock and Stratton Glaciers merge with the surface of the

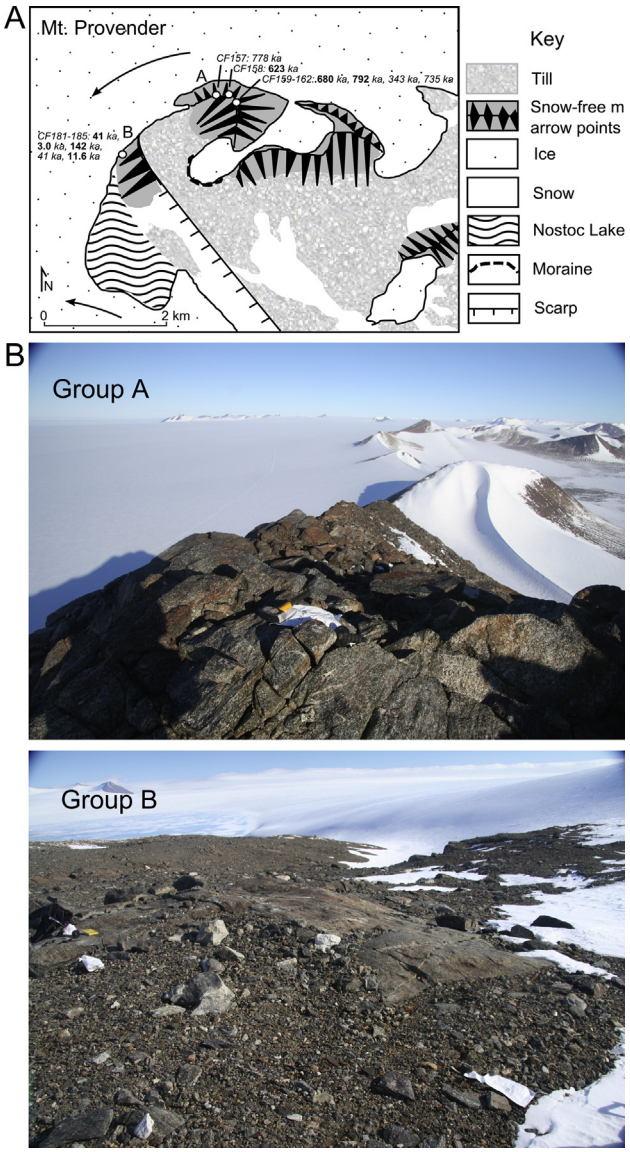


**Fig. 4.** A. Geomorphic map of the Mt. Provender site re-drawn after Höfle and Buggisch (1995). The arrows indicate ice flow direction for Stratton Glacier to the north and Blaiklock Glacier to the south. The letters refer to the groups identified on the basis of their geomorphic characteristics. Sample location and ages are shown; those in bold have relatively simple exposure histories. B. Group A shows iron stained, deeply weathered and pitted rock ($^{10}$Be age range 620–790 ka). The photograph is oriented toward the east, with Mt. Skidmore visible in the distance on the left. Group B shows somewhat iron-stained ice-moulded bedrock and till within 30 m of the ice margin ($^{10}$Be age range: 3–142 ka).

Slessor Glacier (Figs. 2 and 4). The main shear zone at the margin of the Slessor Glacier is situated 15 km NNW of Mt. Provender at an elevation of c. 120 m (RAMP 200 m DEM; Liu et al., 2001).

### 3.1.1. Group A

A bedrock ridge extending down from the summit of Mt. Provender (c. 900 m) to below 600 m where the lowest sample was taken. The samples were taken on the ridge 150–450 m above Stratton Glacier. In many places the gneiss bedrock is iron-stained a deep red colour and is deeply weathered and pitted. Perched boulders were found at some locations (Fig. DR1b). Bedrock and loose blocks have $^{10}$Be exposure ages that range between 620 ka and 790 ka with one exception, a block with an age of 340 ka but with an $^{26}$Al/$^{10}$Be ratio that indicates burial (Fig. DR1). The $^{26}$Al/$^{10}$Be ratios for most other samples can be explained by relatively continuous exposure and erosion, although the ratio of the highest bedrock sample (CF162, 735 ka) would imply that some burial or episodic erosion is likely.

### 3.1.2. Group B

Samples from ice-moulded bedrock and till at the base of Mt. Provender within 20–30 m of the modern ice margin. The bedrock and till are somewhat weathered and iron stained and perched boulders and striated clasts are common. Bedrock and erratic $^{10}$Be exposure ages range between 3 ka and 142 ka and with the exception of one erratic (CF184, 41 ka), the $^{26}$Al/$^{10}$Be ratios suggest relatively simple exposures (Fig. DR2).

## 3.2. Mt. Skidmore

Mt. Skidmore is located 20 km northeast of Mt. Provender where Stratton and Köppen glaciers merge with Slessor Glacier. The main shear zone of Slessor Glacier is situated 12 km NNW of Mt. Skidmore at an elevation of c. 180 m (RAMP 200 m DEM; Liu et al., 2001). Mt. Skidmore is characterised by low-angled, till-covered slopes with polygons, little exposed bedrock and few perched boulders or striated stones. This site is complicated by the presence of small local glaciers which are situated above the sampling sites (Figs. 5 and 6).

### 3.2.1. Group A

A long and narrow bedrock ridge separating Stratton Glacier on the SW side from Ice Tongue A on the NE side. The elevation of the ridge at the sampled locations ranges from c. 830 m–700 m and from near the edge of the ice surface to about 150 m above it. The bedrock is predominantly highly weathered migmatitic gneiss of the Stratton Group (Brommer et al., 1999) which is often fractured with deep red varnish contrasting in places with fresh, more recently eroded surfaces. Where bedrock is not exposed on the ridge top the surfaces are draped by hummocky till or, more often, by small angular debris <10 cm derived from local bedrock and erratics; many of the latter 'ghost boulders' appear as black patches in the field. Few boulders or larger clasts exist on these surfaces.

The $^{10}$Be exposure ages from four erratics and one bedrock sample (CF119) range between 416 ka and 1526 ka. The $^{26}$Al/$^{10}$Be ratios indicate more complex exposure for the three youngest samples close to modern ice and up to 100 m above (Fig. DR3). The oldest age comes from highly weathered bedrock and its $^{26}$Al/$^{10}$Be ratio suggests some erosion or burial; the sample is located just upwind of a wind-drift tail and near to a younger erratic (CF120, 599 ka). The oldest erratic (CF118; 876 ka) is the highest above the modern ice and has a simple exposure history.

### 3.2.2. Group B

A slope below the northwest summit of Mt. Skidmore near to the terminus of the NW trending Ice Tongue A at 600 m elevation. The surface slopes northward in excess of 10° and downslope movement of the sediment is evident in the form of stacked stones and metre-scale gelifluction lobes. The sediment is predominantly composed of thin, flat and dark coloured gravel to cobble-sized clasts of local metabasite which outcrops above the sampled location. A few boulders or larger clasts exist on this surface, and some lighter-coloured angular to sub-rounded clasts were sampled. The $^{10}$Be exposure ages from six erratics range between 151 ka and 625 ka. The three youngest samples have nearly identical $^{26}$Al and $^{10}$Be concentrations which indicate more complex exposures than the three older samples which have simple exposure histories (Fig. DR4).

Please cite this article in press as: Hein, A.S., et al., Geological scatter of cosmogenic-nuclide exposure ages in the Shackleton Range, Antarctica: Implications for glacial history, Quaternary Geochronology (2013), http://dx.doi.org/10.1016/j.quageo.2013.03.008

**Table 2**
Cosmogenic nuclide data.

| Sample ID | Latitude | Longitude | Altitude | Lithology | Type[a] | Thickness | Shielding correction | Quartz mass | $^{10}$Be AMS ID[b] | 10Be concentration[c] ±1σ | $^{26}$Al AMS ID[b] | $^{26}$Al concentration[d] ±1σ |
|---|---|---|---|---|---|---|---|---|---|---|---|---|
| | (dd) | (dd) | (m asl) | | | (cm) | | (G) | | ($10^6$ atom $g^{-1}$[$SiO_2$]) | | ($10^6$ atom $g^{-1}$[$SiO_2$]) |
| Mt Skidmore profile | | | | | | | | | | | | |
| CF_118_08 | −80.32545 | −28.83897 | 825 | Gneiss | E | 4.0 | 0.9992 | 30.015 | b3524 | 8.374 ± 0.189 | a1017 | 44.25 ± 1.49 |
| CF_119_08 | −80.32545 | −28.83897 | 825 | Gneiss | B | 5.0 | 0.9992 | 30.910 | b4512 | 12.50 ± 0.273 | a1298 | 55.05 ± 2.81 |
| CF_120_08 | −80.32436 | −28.85522 | 808 | Gneiss | E | 4.0 | 0.9992 | 30.119 | b4509 | 6.014 ± 0.134 | a1296 | 27.61 ± 1.40 |
| CF_117_08 | −80.32098 | −28.89879 | 748 | Quartzite | E | 3.0 | 0.9992 | 28.433 | b4497 | 5.418 ± 0.121 | a1284 | 25.11 ± 1.4 |
| CF_115_08 | −80.31669 | −28.92190 | 711 | Quartzite | E | 4.0 | 0.9992 | 34.010 | b3528 | 4.000 ± 0.0882 | a1021 | 20.69 ± 0.700 |
| CF_70_08 | −80.29640 | −28.91589 | 605 | Sandstone | E | 5.0 | 0.9954 | 23.550 | b4213 | 1.488 ± 0.0432 | a1184[e] | 8.068 ± 0.423 |
| CF_72_08 | −80.29640 | −28.91589 | 605 | Granite | E | 4.5 | 0.9954 | 29.003 | b3537 | 1.896 ± 0.0448 | a1030 | 11.54 ± 0.443 |
| CF_66_08 | −80.29664 | −28.91595 | 604 | Gneiss | E | 5.0 | 0.9919 | 29.912 | b3540 | 1.376 ± 0.0333 | a1032 | 7.761 ± 0.279 |
| CF_64_08 | −80.29652 | −28.91656 | 598 | Gneiss | E | 5.0 | 0.9919 | 31.427 | b3535 | 1.976 ± 0.0440 | a1028 | 12.03 ± 0.476 |
| CF_78_08 | −80.29568 | −28.90825 | 568 | Sandstone | E | 4.0 | 0.9954 | 42.558 | b3536 | 4.984 ± 0.110 | a1029 | 26.52 ± 0.888 |
| CF_77_08 | −80.29567 | −28.90827 | 564 | Quartzite | E | 5.0 | 0.9954 | 29.941 | b3748 | 1.340 ± 0.0340 | a1130[e] | 7.657 ± 0.040 |
| CF_90_08 | −80.29042 | −28.84511 | 495 | Sandstone | E | 3.5 | 0.9990 | 20.923 | b3816 | 2.825 ± 0.0598 | a1159[e] | 14.30 ± 0.73 |
| CF_91_08 | −80.29042 | −28.84511 | 495 | Conglomerate | E | 5.0 | 0.9990 | 28.435 | b4208 | 2.677 ± 0.0830 | a1180[e] | 12.90 ± 0.676 |
| CF_95_08 | −80.28870 | −28.82594 | 448 | Sandstone | E | 3.5 | 0.9989 | 32.521 | b3772 | 2.594 ± 0.0582 | a1154[e] | 13.75 ± 0.72 |
| CF_36_08 | −80.29020 | −28.67029 | 576 | Quartz | E | 3.0 | 0.9919 | 31.075 | b3833 | 5.669 ± 0.121 | a1177[e] | 34.08 ± 1.74 |
| CF_37_08 | −80.29020 | −28.67029 | 576 | Quartz | E | 4.0 | 0.9919 | 26.262 | b4227 | 7.461 ± 0.216 | a1198[e] | 35.53 ± 1.85 |
| CF_39_08 | −80.28596 | −28.68580 | 508 | Granite | E | 3.5 | 0.9919 | 25.189 | b4209 | 9.820 ± 0.217 | a1182[e] | 37.91 ± 1.95 |
| CF_40_08 | −80.28596 | −28.68580 | 508 | Quartz | E | 5.0 | 0.9919 | 26.938 | b4226 | 5.011 ± 0.150 | a1197[e] | 26.42 ± 1.38 |
| CF_44_08 | −80.28497 | −28.68849 | 474 | Quartz | E | 3.5 | 0.9919 | 31.415 | b4225 | 8.623 ± 0.191 | a1196[e] | 35.66 ± 1.83 |
| CF_45_08 | −80.28497 | −28.68849 | 474 | Quartz | E | 4.0 | 0.9919 | 31.786 | b3758 | 6.475 ± 0.145 | a1140[f] | |
| CF_99_08 | −80.28009 | −28.71314 | 400 | Sandstone | E | 5.0 | 0.9992 | 30.507 | b3771 | 6.126 ± 0.137 | a1153 | 36.61 ± 1.88 |
| CF_100_08 | −80.28009 | −28.71314 | 400 | Sandstone | E | 5.0 | 0.9992 | 31.852 | b3541 | 5.438 ± 0.120 | a1034 | 29.66 ± 0.997 |
| CF_52_08 | −80.27970 | −28.70647 | 399 | Sandstone | E | 2.0 | 0.9919 | 32.871 | b3757 | 8.359 ± 0.187 | a1137[e] | 40.96 ± 2.10 |
| CF_53_08 | −80.27970 | −28.70647 | 399 | Sandstone | E | 5.0 | 0.9919 | 33.235 | b3760 | 4.732 ± 0.106 | a1142[e] | 22.10 ± 1.14 |
| CF_105_08 | −80.27822 | −28.71603 | 382 | Quartzite | E | 5.0 | 0.9992 | 32.421 | b3530 | 7.451 ± 0.164 | a1023 | 45.61 ± 1.52 |
| CF_104_08 | −80.27812 | −28.71819 | 380 | Sandstone | E | 5.0 | 0.9992 | 31.600 | b3534 | 6.200 ± 0.137 | a1025 | 32.58 ± 1.10 |
| CF_196_08 | −80.27249 | −28.71008 | 363 | Sandstone | E | 5.0 | 0.9968 | 25.469 | b3529 | 4.437 ± 0.0984 | a1022 | 22.80 ± 0.766 |
| CF_108_08 | −80.27386 | −28.73442 | 339 | Quartz | E | 5.0 | 0.9992 | 29.075 | b3539 | 3.886 ± 0.0889 | a1031 | 24.32 ± 0.815 |
| CF_110_08 | −80.27386 | −28.73442 | 339 | Sandstone | E | 3.0 | 0.9992 | 29.403 | b3770 | 6.063 ± 0.136 | a1152[f] | |
| CF_200_08 | −80.27017 | −28.71768 | 335 | Gneiss | E | 3.5 | 0.9968 | 22.759 | b4221 | 3.491 ± 0.108 | a1193[e] | 18.17 ± 0.94 |
| CF_202_08 | −80.27017 | −28.71768 | 335 | Gneiss | E | 3.0 | 0.9968 | 19.048 | b3821 | 3.614 ± 0.0794 | a1165[e] | 17.81 ± 0.93 |
| CF_138B_08 | −80.27471 | −28.77463 | 324 | Quartzite | E | 4.5 | 0.9997 | 29.605 | b3769 | 4.749 ± 0.106 | a1149[e] | 21.37 ± 1.10 |
| CF_139_08 | −80.27469 | −28.77379 | 323 | Granite | E | 4.5 | 0.9997 | 27.581 | b3751 | 2.349 ± 0.0526 | a1131[e] | 13.51 ± 0.70 |
| CF_142_08 | −80.27397 | −28.77537 | 309 | Sandstone | E | 4.0 | 0.9997 | 26.553 | b3830 | 3.929 ± 0.0876 | a1173[e] | 24.33 ± 1.26 |
| CF_143_08 | −80.27383 | −28.77680 | 308 | Granite | E | 4.5 | 0.9997 | 25.050 | b4224 | 4.646 ± 0.135 | a1195[e] | 22.36 ± 1.15 |
| CF_150_08 | −80.27216 | −28.77998 | 284 | Sandstone | E | 5.0 | 0.9998 | 34.188 | b3759 | 2.389 ± 0.0536 | a1141[e] | 11.10 ± 0.58 |
| CF_147_08 | −80.27216 | −28.77998 | 284 | Sandstone | E | 5.0 | 0.9997 | 30.776 | b3763 | 3.070 ± 0.0688 | a1143[e] | 16.24 ± 0.85 |
| CF_155_08 | −80.27158 | −28.78135 | 279 | Gneiss | E | 3.5 | 0.9998 | 22.303 | b3752 | 2.232 ± 0.0500 | a1132[e] | 12.53 ± 0.73 |
| CF_154_08 | −80.27147 | −28.78090 | 276 | Quartz | E | 5.0 | 0.9998 | 32.848 | b4214 | 3.346 ± 0.104 | a1185[e] | 15.90 ± 0.83 |
| CF_56_08 | −80.24772 | −28.75172 | 326 | Gneiss | E | 4.0 | 0.9919 | 24.210 | b4496 | 0.8548 ± 0.0208 | a1283 | 5.375 ± 0.301 |
| CF_57_08 | −80.26012 | −28.85200 | 278 | Granite | E | 3.5 | 0.9919 | 28.128 | b3746 | 2.307 ± 0.0549 | a1128[f] | |
| CF_58A_08 | −80.26012 | −28.85200 | 278 | Gneiss | E | 3.5 | 0.9919 | 27.906 | b3747 | 0.1911 ± 0.00642 | a1129[e] | 0.846 ± 0.041 |
| CF_58B_08 | −80.26012 | −28.85200 | 278 | Gneiss | E | 3.5 | 0.9919 | 13.410 | b4504 | 0.1868 ± 0.00719 | a1290 | 0.828 ± 0.062 |
| CF_59_08 | −80.26188 | −28.84317 | 268 | Quartz | E | 5.5 | 0.9919 | 28.214 | b4502 | 1.240 ± 0.0303 | a1288 | 6.608 ± 0.362 |
| CF_60_08 | −80.26188 | −28.84317 | 268 | Gneiss | E | 5.0 | 0.9919 | 26.752 | b4500 | 5.495 ± 0.122 | a1285 | 26.71 ± 1.36 |
| Mt. Sheffield profile | | | | | | | | | | | | |
| CF_207_08 | −80.11722 | −25.78078 | 474 | Sandstone | E | 4.0 | 0.9859 | 34.912 | b3775 | 2.175 ± 0.0488 | a1155[e] | 13.30 ± 0.68 |
| CF_204_08 | −80.11717 | −25.77962 | 474 | Quartzite | E | 3.5 | 0.9859 | 25.841 | b3827 | 5.195 ± 0.115 | a1170[e] | 29.77 ± 1.52 |
| CF_205_08 | −80.11722 | −25.78078 | 474 | Sandstone | E | 3.5 | 0.9859 | 25.806 | b3832 | 5.694 ± 0.121 | a1176[f] | |
| CF_208_08 | −80.11722 | −25.78078 | 474 | Quartzite | E | 5.0 | 0.9859 | 28.817 | b3829 | 4.820 ± 0.107 | a1172[e] | 30.35 ± 1.55 |
| CF_206_08 | −80.11722 | −25.78078 | 474 | Volcanic | E | 4.5 | 0.9859 | 4.775 | b4215 | 2.095 ± 0.0698 | a1186[e] | 14.49 ± 0.79 |
| CF_209_08 | −80.11571 | −25.78073 | 429 | Sandstone | E | 3.5 | 0.9859 | 29.565 | b3828 | 1.535 ± 0.0339 | a1171[e] | 11.71 ± 0.62 |
| CF_211_08 | −80.11574 | −25.78122 | 427 | Quartz | E | 4.0 | 0.9859 | 31.215 | b3764 | 4.017 ± 0.0900 | a1144[e] | 17.97 ± 0.92 |
| CF_210_08 | −80.11574 | −25.78122 | 427 | Schist | E | 4.0 | 0.9859 | 23.167 | b4212 | 0.8842 ± 0.0284 | a1183[e] | 4.056 ± 0.230 |
| CF_212_08 | −80.11574 | −25.78122 | 427 | Quartzite | E | 3.0 | 0.9859 | 29.001 | b4220 | 5.623 ± 0.169 | a1192[f] | |
| CF_213A_08 | −80.11532 | −25.78703 | 406 | Quartzite | E | 5.0 | 0.9859 | 23.352 | b3525 | 1.023 ± 0.0234 | a1018 | 8.389 ± 0.288 |
| CF_213B_08 | −80.11532 | −25.78703 | 406 | Quartzite | E | 6.0 | 0.9859 | 24.134 | b4508 | 1.282 ± 0.312 | a1295 | 8.415 ± 0.463 |
| CF_214_08 | −80.11532 | −25.78703 | 406 | Quartzite | E | 4.0 | 0.9859 | 24.427 | b3527 | 0.8398 ± 0.0201 | a1019[f] | |
| CF_215A_08 | −80.11352 | −25.78313 | 309 | Gneiss | E | 3.0 | 0.9857 | 28.415 | b3818 | 0.1653 ± 0.0564 | a1161[e] | 0.751 ± 0.052 |
| CF_215B_08 | −80.11352 | −25.78313 | 309 | Gneiss | E | 3.0 | 0.9857 | 20.871 | b4506 | 0.1730 ± 0.00643 | a1293 | 0.984 ± 0.061 |
| CF_217_08 | −80.11352 | −25.78313 | 309 | Gneiss | E | 3.0 | 0.9857 | 14.927 | b4219 | 2.633 ± 0.0816 | a1191[e] | 13.82 ± 0.72 |
| CF_216_08 | −80.11352 | −25.78313 | 309 | Quartzite | E | 3.0 | 0.9857 | 18.940 | b3819 | 0.02250 ± 0.00212 | a1164[e] | 0.253 ± 0.021 |
| CF_220_08 | −80.11286 | −25.78762 | 310 | Gneiss | E | 3.5 | 0.9857 | 20.761 | b3817 | 0.1824 ± 0.00630 | a1160[e] | 1.584 ± 0.106 |
| Mt. Provender profile | | | | | | | | | | | | |
| CF_162_08 | −80.38188 | −29.95333 | 913 | Granite | B | 2.5 | 0.9982 | 24.641 | b3765 | 7.943 ± 0.178 | a1146[e] | 35.84 ± 1.83 |
| CF_160_08 | −80.38144 | −29.95613 | 893 | Gneiss | B | 4.5 | 0.9982 | 26.710 | b4216 | 8.152 ± 0.230 | a1189[e] | 42.29 ± 2.15 |
| CF_161_08 | −80.38144 | −29.95613 | 893 | Gneiss | E | 4.0 | 0.9982 | 24.420 | b3767 | 3.945 ± 0.0886 | a1148[e] | 10.40 ± 0.53 |
| CF_159_08 | −80.38144 | −29.95613 | 893 | Gneiss | E | 5.0 | 0.9982 | 21.310 | b3754 | 7.163 ± 0.160 | a1135[e] | 38.45 ± 1.96 |
| CF_158_08 | −80.37932 | −29.97815 | 744 | Granodiorite | B | 4.5 | 0.9978 | 23.599 | b3753 | 5.834 ± 0.131 | a1134[e] | 30.49 ± 1.56 |

Please cite this article in press as: Hein, A.S., et al., Geological scatter of cosmogenic-nuclide exposure ages in the Shackleton Range, Antarctica: Implications for glacial history, Quaternary Geochronology (2013), http://dx.doi.org/10.1016/j.quageo.2013.03.008

**Table 2** (*continued*)

| Sample ID | Latitude | Longitude | Altitude | Lithology | Type[a] | Thickness | Shielding correction | Quartz mass | $^{10}$Be AMS ID[b] | 10Be concentration[c] $\pm1\sigma$ | $^{26}$Al AMS ID[b] | $^{26}$Al concentration[d] $\pm1\sigma$ |
|---|---|---|---|---|---|---|---|---|---|---|---|---|
| | (dd) | (dd) | (m asl) | | | (cm) | | (G) | | ($10^6$ atom g$^{-1}$[SiO$_2$]) | | ($10^6$ atom g$^{-1}$[SiO$_2$]) |
| CF_157_08 | −80.37860 | −29.99452 | 600 | Gneiss | B | 4.5 | 0.9978 | 23.415 | b3823 | 6.157 ± 0.137 | a1167[e] | 44.23 ± 2.26 |
| CF_184_08 | −80.38455 | −30.06789 | 239 | Gneiss | E | 4.5 | 0.9968 | 31.154 | b3776 | 0.2714 ± 0.00915 | a1156[e] | 0.902 ± 0.073 |
| CF_185_08 | −80.38455 | −30.06789 | 239 | Granodiorite | B | 3.5 | 0.9968 | 22.958 | b3822 | 0.07846 ± 0.00316 | a1166[e] | 0.477 ± 0.034 |
| CF_181_08 | −80.38455 | −30.06789 | 239 | Granodiorite | B | 5.0 | 0.9968 | 14.224 | b4507 | 0.2725 ± 0.00933 | a1294 | 2.034 ± 0.133 |
| CF_182_08 | −80.38455 | −30.06789 | 239 | Gneiss | E | 2.5 | 0.9968 | 13.370 | b4495 | 0.02031 ± 0.00351 | a1282 | 0.2143 ± 0.039 |
| CF_183_08 | −80.38455 | −30.06789 | 239 | Gneiss | E | 5.0 | 0.9968 | 24.510 | b4501 | 0.9227 ± 0.0277 | a1287 | 5.989 ± 0.347 |

$^{10}$Be data previously reported (Hein et al., 2011).

[a] Bedrock (B); Erratic cobble (E).

[b] AMS measurements made at Scottish Universities Environmental Research Centre (SUERC).

[c] Normalised to NIST SRM-4325 Be standard material with a revised nominal $^{10}$Be/$^{9}$Be ratio ($2.79 \times 10^{-11}$) (Nishiizumi et al., 2007) and half-life of 1.387 Ma (Chmeleff et al., 2010; Korschinek et al., 2010) and corrected for process blanks; uncertainties include propagated AMS sample/lab-blank uncertainty and a 2% carrier mass uncertainty.

[d] Normalised to the Purdue Z92-0222 Al standard material with a nominal $^{26}$Al/$^{27}$Al ratio of $4.11 \times 10^{-11}$ that agrees with Al standard material of Nishiizumi. (2004), and corrected for process blanks; uncertainties include propagated AMS sample/lab-blank uncertainty and a 5% stable $^{27}$Al measurement (ICP-OES) uncertainty.

[e] ICP re-measured (see supplementary discussion).

[f] ICP could not be re-measured.

### 3.2.3. Group C

Near to a presently snow-filled gully marking a former melt-water route extending from Ice Tongues A and B at 500–450 m. The surface slopes northward at up to 10° and there is evidence for sediment churning with stacked and vertically oriented stones at the margins of polygons. The till is composed of sand to boulder-sized clasts of sub-angular gneisses, quartzites and sandstones. The overall degree of weathering is low and this is reflected in the grey colour of the till which, in places, overlies fine sediments. The $^{10}$Be exposure ages from three erratics range between 337 ka and 352 ka. The samples have nearly identical $^{26}$Al and $^{10}$Be concentrations, which indicate complex exposures (Fig. DR5). This is the tightest cluster of exposure ages from a single group on Mt. Skidmore.

### 3.2.4. Group D

Further east at a location north of Ice Tongue B and northwest of the snow-drift glacier on the eastern side of the massif between 575 m and 380 m elevation. The sampled surfaces are relatively flat with ~15 m diameter tundra polygons with depressed margins. The till is pink in colour and is predominantly composed of <10 cm angular clasts of sandstone, quartz, quartzite, and gneiss. The sediment is highly weathered as evidenced by the degree of rock varnish, the few up-standing stones outside polygon margins, the abundance of ghost boulders that have disintegrated in situ, and the near-complete lack of surface boulders particularly at the southernmost site. The $^{10}$Be exposure ages from twelve erratics range between 680 ka and 1640 ka. The $^{26}$Al/$^{10}$Be ratios mainly show a wide spread of simple exposure histories (Fig. 9 and DR6).

### 3.2.5. Group E

Surfaces on or near moraines on the northeast shoulder of the massif between 360 and 330 m. The till in this area is mainly composed of weathered gravel to cobble-sized, angular to sub-angular clasts, some of which have fractured in situ. The colour of the till changes from pink in the west to more grey towards the east. Sediment movement is evident by fractured boulder fragments that are aligned downslope. The $^{10}$Be exposure ages from five erratics range between 531 ka and 1024 ka. One sample (CF108) has an $^{26}$Al/$^{10}$Be ratio indicating continuous exposure since c. 605 ka (Fig. 9 and DR7); the remainder show more complex exposures.

### 3.2.6. Group F

Gentle slopes at the lowest elevation (325–280 m) on Mt. Skidmore. The slopes are up to 50 m above an ice-covered lake dammed by the glacier. The character of the till varies throughout the sampled area but is typically grey to pink in colour and includes many frost-shattered boulders and polygons with deep margins. While weathered boulders and larger clasts are relatively abundant up-slope (south), they are almost entirely absent at the lowest elevation near the lake where the till has a flattened appearance. A series of horizontal lake terraces exist in this latter area. The $^{10}$Be exposure ages from eight erratics range between 348 ka and 778 ka. One sample (CF142) has an $^{26}$Al/$^{10}$Be ratio indicating relatively continuous exposure since c. 630 ka and this sample together with CF143 (772 ka) come from a stable part of the surface (Fig. 9 and DR8); the remainder show more complex exposures.

### 3.2.7. Group G

The modern moraine (325–270 m) which dams the lake on the north side of the massif. The till is grey in colour, the clasts are angular to sub-angular and most of the larger clasts are gneisses with less sandstone than at sites up slope. There is abundant fine material and several of the boulders and larger clasts are vertically oriented. The $^{10}$Be exposure ages from five erratics range between 27 ka and 1016 ka. The $^{26}$Al/$^{10}$Be ratios imply relatively simple exposure for the oldest sample (Fig. 9 and DR9). A second sample (CF56) also has a relatively simple exposure with a $^{10}$Be age of 120 ka. The youngest sample was measured twice resulting in consistent $^{26}$Al and $^{10}$Be concentrations and ratios indicating burial.

## 3.3. Mt. Sheffield

Mt. Sheffield is situated on the main shear zone of the Slessor Glacier at an elevation of c. 310 m and 60 km upstream of Mt. Skidmore. Clear lateral trim-lines are present at elevations of up to 165 m above the modern ice margin (Fig. 7).

### 3.3.1. Group A

The uppermost sampled till on Mt. Sheffield is weathered and pink in colour. Most clasts are angular to sub-angular in shape and mostly sand to coarse pebble in size; the clasts are underlain by fines. Several larger cobbles and boulders are scattered across the surface; many are fractured with fragments aligned down-slope. The lithologies include quartz, quartzite, granite, gneiss, schist, and volcanics. The $^{10}$Be exposure ages from five erratics range between 267 ka and 822 ka with clusters at 270 ka and c. 700 ka. The $^{26}$Al/$^{10}$Be ratios imply simple exposure histories (Fig. DR10).

### 3.3.2. Group B

Till surface lower in elevation and with a larger average clast size (large pebble to cobble sizes), and a grey-pink colour. The $^{10}$Be

Please cite this article in press as: Hein, A.S., et al., Geological scatter of cosmogenic-nuclide exposure ages in the Shackleton Range, Antarctica: Implications for glacial history, Quaternary Geochronology (2013), http://dx.doi.org/10.1016/j.quageo.2013.03.008

**Table 3**
Surface exposure ages.

| Site | Sample ID | Altitude | $^{10}$Be age[a] ±1σ (int)[b] | ±1σ (ext)[b] | $^{26}$Al age[a] ±1σ (int) | ±1σ (ext)[b] | $^{26}$Al/$^{10}$Be[c] ±1σ |
|---|---|---|---|---|---|---|---|
| | | (m asl) | (ka) | (ka) | (ka) | (ka) | |
| Mt Skidmore profile | | | | | | | |
| *Group A* | CF_118_08 | 825 | 876.4 ± 23.0 | 131 | 798.1 ± 36.1 | 156 | 5.29 ± 0.30 |
| | CF_119_08 | 825 | 1526 ± 45.2 | 273 | 1165 ± 95.9 | 279.00 | 4.40 ± 0.24 |
| | CF_120_08 | 808 | 598.9 ± 14.5 | 83.4 | 429.5 ± 25.2 | 68.40 | 4.59 ± 0.25 |
| | CF_117_08 | 748 | 559.9 ± 13.5 | 77.2 | 404.4 ± 25.7 | 64.50 | 4.63 ± 0.28 |
| | CF_115_08 | 711 | 416.4 ± 9.59 | 55.3 | 336.8 ± 19.5 | 51.3 | 5.17 ± 0.29 |
| *Group B* | CF_70_08 | 605 | 162.6 ± 4.65 | 20.5 | 133.1 ± 7.03 | 18.3 | 5.42 ± 0.32 |
| | CF_72_08 | 605 | 208.6 ± 4.90 | 26.3 | 195.3 ± 11.2 | 28 | 6.09 ± 0.37 |
| | CF_66_08 | 604 | 150.5 ± 3.58 | 18.7 | 128.3 ± 6.94 | 17.7 | 5.64 ± 0.33 |
| | CF_64_08 | 598 | 221.2 ± 4.91 | 27.9 | 207.7 ± 12.2 | 30 | 6.09 ± 0.37 |
| | CF_78_08 | 568 | 625.4 ± 15.1 | 87.7 | 543.4 ± 34.3 | 92.3 | 5.32 ± 0.30 |
| | CF_77_08 | 564 | 151.7 ± 3.78 | 18.9 | 131.1 ± 6.91 | 18 | 5.71 ± 0.33 |
| *Group C* | CF_90_08 | 495 | 352.8 ± 7.67 | 46 | 275.1 ± 15.1 | 40.5 | 5.06 ± 0.28 |
| | CF_91_08 | 495 | 337.1 ± 10.7 | 44.6 | 248.1 ± 13.8 | 36.1 | 4.82 ± 0.29 |
| | CF_95_08 | 448 | 337.5 ± 7.75 | 43.9 | 277.0 ± 15.5 | 40.9 | 5.30 ± 0.30 |
| *Group D* | CF_36_08 | 576 | 718.3 ± 17.1 | 103 | 758.3 ± 51.7 | 144 | 6.01 ± 0.33 |
| | CF_37_08 | 576 | 1023 ± 35.5 | 161 | 817.5 ± 58.2 | 161 | 4.76 ± 0.28 |
| | CF_39_08 | 508 | 1637 ± 49.8 | 303 | 997.9 ± 76.4 | 217 | 3.86 ± 0.22 |
| | CF_40_08 | 508 | 681.6 ± 22.5 | 98.4 | 591.6 ± 38.2 | 103 | 5.27 ± 0.32 |
| | CF_44_08 | 474 | 1414 ± 41.1 | 246 | 950.0 ± 70.9 | 201 | 4.14 ± 0.23 |
| | CF_45_08 | 474 | 963.2 ± 25.5 | 148 | | | |
| | CF_99_08 | 400 | 983.0 ± 26.1 | 152 | 1133 ± 91.9 | 267 | 5.98 ± 0.33 |
| | CF_100_08 | 400 | 845.3 ± 21.5 | 126 | 799.5 ± 56.8 | 156 | 5.45 ± 0.31 |
| | CF_52_08 | 399 | 1474 ± 43.8 | 260.3 | 1369 ± 123 | 370 | 4.90 ± 0.27 |
| | CF_53_08 | 399 | 720.4 ± 18.0 | 104 | 534.9 ± 33.4 | 90.3 | 4.67 ± 0.26 |
| | CF_105_08 | 382 | 1310 ± 36.9 | 221 | 1941 ± 224 | 750 | 6.12 ± 0.35 |
| | CF_104_08 | 380 | 1024 ± 27.1 | 160 | 956.7 ± 73.1 | 204 | 5.26 ± 0.30 |
| *Group E* | CF_196_08 | 363 | 690.5 ± 17.0 | 98.5 | 579.5 ± 37.3 | 100 | 5.14 ± 0.29 |
| | CF_108_08 | 339 | 605.2 ± 15.1 | 84.5 | 651.3 ± 43.3 | 117 | 6.26 ± 0.36 |
| | CF_110_08 | 339 | 1024 ± 27.5 | 160 | | | |
| | CF_200_08 | 335 | 531.0 ± 17.7 | 73.8 | 440.3 ± 26.3 | 70.6 | 5.21 ± 0.31 |
| | CF_202_08 | 335 | 550.0 ± 13.0 | 75.6 | 427.2 ± 25.8 | 68.2 | 4.93 ± 0.28 |
| *Group F* | CF_138B_08 | 324 | 778.4 ± 19.8 | 114 | 553.7 ± 34.6 | 94.3 | 4.50 ± 0.25 |
| | CF_139_08 | 323 | 347.6 ± 8.00 | 45.4 | 314.0 ± 17.9 | 47.2 | 5.75 ± 0.33 |
| | CF_142_08 | 309 | 627.8 ± 15.3 | 88.1 | 670.6 ± 44.6 | 122 | 6.19 ± 0.35 |
| | CF_143_08 | 308 | 772.3 ± 25.4 | 114 | 601.0 ± 38.3 | 105 | 4.81 ± 0.28 |
| | CF_150_08 | 284 | 370.5 ± 8.59 | 48.6 | 262.4 ± 14.6 | 38.4 | 4.65 ± 0.26 |
| | CF_147_08 | 284 | 490.0 ± 11.7 | 66.4 | 411.4 ± 24.7 | 65.2 | 5.29 ± 0.30 |
| | CF_155_08 | 279 | 341.2 ± 7.86 | 44.5 | 299.0 ± 18.9 | 45.6 | 5.61 ± 0.35 |
| | CF_154_08 | 276 | 545.9 ± 18.2 | 76.2 | 405.1 ± 24.1 | 63.9 | 4.75 ± 0.29 |
| *Group G* | CF_56_08 | 326 | 119.7 ± 2.8 | 14.8 | 113.6 ± 6.4 | 15.60 | 6.29 ± 0.38 |
| | CF_57_08 | 278 | 357.1 ± 8.77 | 46.8 | | | |
| | CF_58A_08 | 278 | 27.29 ± 0.877 | 3.36 | 17.8 ± 1.02 | 2.37 | 4.43 ± 0.30 |
| | CF_58B_08 | 278 | 26.7 ± 1.0 | 3.3 | 17.4 ± 1.3 | 2.50 | 4.43 ± 0.37 |
| | CF_59_08 | 268 | 189.2 ± 4.6 | 23.8 | 152.4 ± 8.5 | 21.30 | 5.33 ± 0.32 |
| | CF_60_08 | 268 | 1016 ± 30.0 | 158 | 835.4 ± 59.1 | 166.00 | 4.86 ± 0.27 |
| Mt. Sheffield profile | | | | | | | |
| *Group A* | CF_207_08 | 474 | 276.8 ± 6.27 | 35.5 | 264.3 ± 14.5 | 38.7 | 6.12 ± 0.34 |
| | CF_204_08 | 474 | 734.6 ± 18.2 | 106 | 725.5 ± 48.7 | 135 | 5.73 ± 0.32 |
| | CF_205_08 | 474 | 821.6 ± 19.9 | 121 | | | |
| | CF_208_08 | 474 | 681.3 ± 16.8 | 97.0 | 760.0 ± 51.7 | 145 | 6.30 ± 0.35 |
| | CF_206_08 | 474 | 267.0 ± 8.96 | 34.9 | 293.1 ± 17.3 | 44 | 6.92 ± 0.44 |
| *Group B* | CF_209_08 | 429 | 199.2 ± 4.36 | 25.0 | 238.9 ± 13.4 | 34.7 | 7.63 ± 0.44 |
| | CF_211_08 | 427 | 573.6 ± 13.9 | 79.4 | 396.6 ± 22.9 | 62.1 | 4.47 ± 0.25 |
| | CF_210_08 | 427 | 112.9 ± 3.53 | 14.2 | 77.0 ± 4.3 | 10.4 | 4.59 ± 0.30 |
| | CF_212_08 | 427 | 849.9 ± 29.4 | 128 | | | |
| *Group C* | CF_213A_08 | 406 | 135.1 ± 3.02 | 16.7 | 171.4 ± 9.26 | 24 | 8.20 ± 0.47 |
| | CF_213B_08 | 406 | 172.3 ± 4.1 | 21.6 | 173.5 ± 9.8 | 24.50 | 6.56 ± 0.40 |
| | CF_214_08 | 406 | 109.3 ± 2.54 | 13.5 | | | |
| *Group D* | CF_215A_08 | 309 | 22.95 ± 0.747 | 2.82 | 15.4 ± 1.0 | 2.1 | 4.54 ± 0.35 |
| | CF_215B_08 | 309 | 24.0 ± 0.9 | 3.00 | 20.2 ± 1.2 | 2.70 | 5.69 ± 0.41 |
| | CF_217_08 | 309 | 400.8 ± 12.9 | 53.9 | 328.2 ± 18.9 | 49.8 | 5.25 ± 0.32 |
| | CF_216_08 | 309 | 3.115 ± 0.278 | 0.469 | 5.2 ± 0.4 | 0.7 | 11.24 ± 1.41 |
| | CF_220_08 | 310 | 25.41 ± 0.839 | 3.13 | 32.8 ± 2.1 | 4.5 | 8.69 ± 0.65 |
| Mt. Provender profile | | | | | | | |
| *Group A* | CF_162_08 | 913 | 734.9 ± 18.6 | 106 | 523.6 ± 32.3 | 87.6 | 4.51 ± 0.25 |
| | CF_160_08 | 893 | 791.5 ± 25.5 | 117 | 688.0 ± 45.6 | 126 | 5.19 ± 0.30 |
| | CF_161_08 | 893 | 342.8 ± 7.93 | 44.7 | 130.6 ± 6.78 | 17.8 | 2.64 ± 0.15 |
| | CF_159_08 | 893 | 680.3 ± 17.0 | 96.8 | 605.8 ± 38.7 | 106 | 5.37 ± 0.30 |
| | CF_158_08 | 744 | 623.1 ± 15.3 | 87.4 | 528.9 ± 32.7 | 88.8 | 5.23 ± 0.29 |
| | CF_157_08 | 600 | 778.4 ± 19.6 | 114 | 1131 ± 91.0 | 265 | 7.18 ± 0.40 |

Please cite this article in press as: Hein, A.S., et al., Geological scatter of cosmogenic-nuclide exposure ages in the Shackleton Range, Antarctica: Implications for glacial history, Quaternary Geochronology (2013), http://dx.doi.org/10.1016/j.quageo.2013.03.008

**Table 3** (*continued*)

| Site | Sample ID | Altitude (m asl) | $^{10}$Be age[a] ±1σ (int)[b] (ka) | ±1σ (ext)[b] (ka) | $^{26}$Al age[a] ±1σ (int) (ka) | ±1σ (ext)[b] (ka) | $^{26}$Al/$^{10}$Be[c] ±1σ |
|---|---|---|---|---|---|---|---|
| *Group B* | CF_184_08 | 239 | 40.52 ± 1.31 | 5 | 19.8 ± 1.5 | 2.9 | 3.32 ± 0.29 |
| | CF_185_08 | 239 | 11.55 ± 0.443 | 1.44 | 10.4 ± 0.7 | 1.4 | 6.08 ± 0.50 |
| | CF_181_08 | 239 | 40.9 ± 1.3 | 5.00E+00 | 45.4 ± 2.9 | 6.20 | 7.46 ± 0.55 |
| | CF_182_08 | 239 | 3.0 ± 0.5 | 6.00E-01 | 4.6 ± 0.8 | 1.00 | 10.55 ± 2.66 |
| | CF_183_08 | 239 | 141.8 ± 4.2 | 1.78E+01 | 140.0 ± 8.2 | 19.60 | 6.49 ± 0.42 |

[a] Ages calculated with v.2.2 of the CRONUS-Earth exposure age calculator (main calculator v.2.1; constants v.2.2.1; muons v.1.1)(Balco et al., 2008). Dunai (2001) scaling, no erosion correction. Age sensitivity to scaling model <6–8% (Desilets et al., 2006; Lal, 1991; Lifton et al., 2005; Stone, 2000).
[b] (int) = internal analytical uncertainties; (ext) = propagated external uncertainties for scaling and production of cosmogenic nuclides.
[c] Production rate ratio is 6.75.

exposure ages from four erratics range between 113 ka and 850 ka. The $^{26}$Al/$^{10}$Be ratios indicate a simple exposure history for sample CF209 (c. 200 ka) and complex exposure for CF210 and CF211 (113 ka and 574 ka). Sample CF210 comes from a shattered boulder and is likely to be erroneously young (Fig. DR11).

### 3.3.3. Group C

Within a clearly defined moraine draped in large angular boulders embedded in sands and gravels with relatively few perched boulders. The lithology is predominantly gneiss that is weathered to varying degrees and colours. The $^{10}$Be exposure ages from two erratics are 109 ka and 172 ka. The only available $^{26}$Al/$^{10}$Be ratio indicates a simple exposure history for sample CF213 at 172 ka (Fig. DR12).

### 3.3.4. Group D

Near the ice margin in an area dense in angular cobbles and boulders with little or no fine material. This is an area with shattered clasts and a nearby ice-cored moraine. The $^{10}$Be exposure ages from four erratics range between 3 ka and 401 ka. The available $^{26}$Al/$^{10}$Be ratios indicate simple exposure histories (Fig. DR13).

### 3.4. PCA results

Fig. 8 presents the PCA results for each site. The results from Mt. Provender are intuitive and expected; they show a first order correlation between age, elevation and degree of weathering, which increase together. In other words, the highest samples are most weathered and have the oldest exposure ages, while the lower samples are less weathered and have the youngest exposure ages.

The exposure age results from the larger Mt. Skidmore prompted this investigation because they are the most numerous and complicated of the three sites (Fig. 8). Yet despite the complexity it is reassuring to find that basic fundamental correlations do exist. A key correlation exists between the degree of weathering and the exposure age, which increase and decrease together. A second rather obvious correlation exists between surface slope and degree of stability; the steeper the slope the greater the signs of instability, for example gelifluction lobes. These indices of instability are inversely correlated with age and weathering such that the oldest, most weathered samples are found on flat stable surfaces, and younger, least weathered samples are correlated with sites with evidence of instability. Another inverse correlation exists between age/weathering and exposure history, with young, unweathered

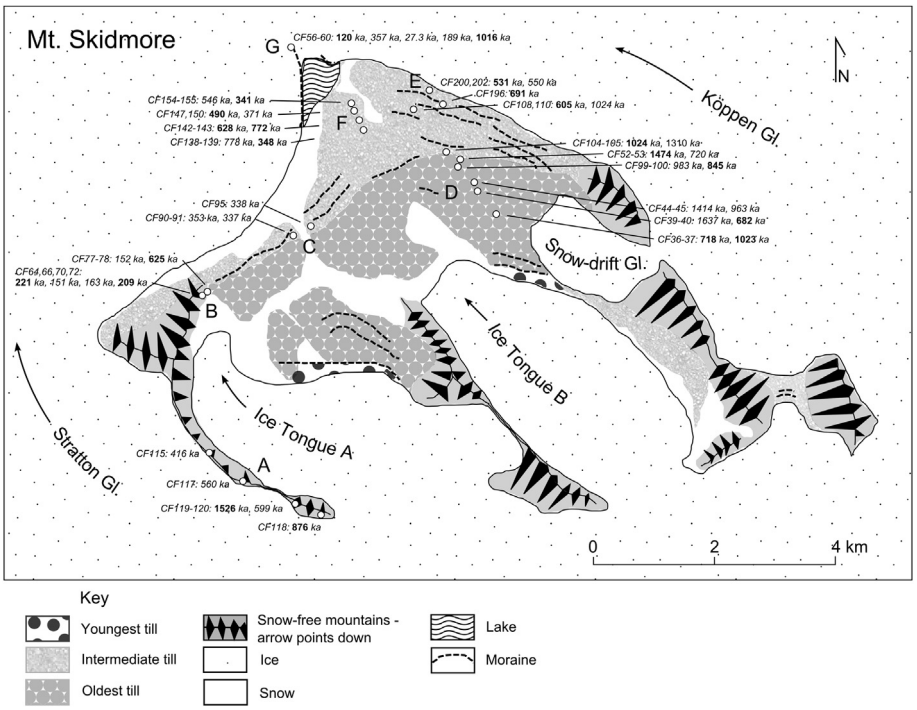


**Fig. 5.** Geomorphic map of the Mt. Skidmore site re-drawn after Höfle and Buggisch (1995). The arrows indicate ice flow directions. The letters refer to the geomorphic groups. Sample location and ages are shown; those in bold have relatively simple exposure histories.

Please cite this article in press as: Hein, A.S., et al., Geological scatter of cosmogenic-nuclide exposure ages in the Shackleton Range, Antarctica: Implications for glacial history, Quaternary Geochronology (2013), http://dx.doi.org/10.1016/j.quageo.2013.03.008


**Fig. 6.** Mt. Skidmore geomorphic groups: A. Highly weathered gneiss and till with occasional erratics ($^{10}$Be age range: 416–1526 ka). B. Intermediate till surface disturbed by gelifluction deposits ($^{10}$Be age range: 157–625 ka). C. Churned till surface near an ice covered gully ($^{10}$Be age range:337–352 ka). D. Stable pink-coloured, small-sized till surface ($^{10}$Be age range: 680–1640 ka). E. Pink-grey till with some periglacial disturbance ($^{10}$Be age range: 531–1024 ka) F. Grey-pink till at low altitudes with large cobbles at polygon boundaries ($^{10}$Be age range: 348–778 ka). G. The modern moraine on the ice surface ($^{10}$Be age range: 27–1016 ka).

clasts more often having complex exposure histories than older weathered clasts. Interestingly, samples with complex exposures are more common on active surfaces.

The PCA results from Mt. Sheffield show a correlation with the degree of weathering which increases with age/elevation.

## 4. Interpreting the glacial history

There is a great deal of geological scatter evident in the exposure age results (Fig. 9 and DR1-13). Despite this there remains enough consistency in the data to draw some conclusions on the glacial history in this region and to speculate on specific processes that have operated in the past. Many of these findings would not have been possible using a single nuclide approach.

### 4.1. Mt. Provender

The $^{26}$Al and $^{10}$Be concentrations in bedrock on the summit of Mt. Provender indicate that the last significant erosion of this surface took place probably several million years ago. The $^{26}$Al/$^{10}$Be ratio indicates a more complex exposure history than observed on bedrock lower down the ridge. The summit bedrock is less iron

Please cite this article in press as: Hein, A.S., et al., Geological scatter of cosmogenic-nuclide exposure ages in the Shackleton Range, Antarctica: Implications for glacial history, Quaternary Geochronology (2013), http://dx.doi.org/10.1016/j.quageo.2013.03.008

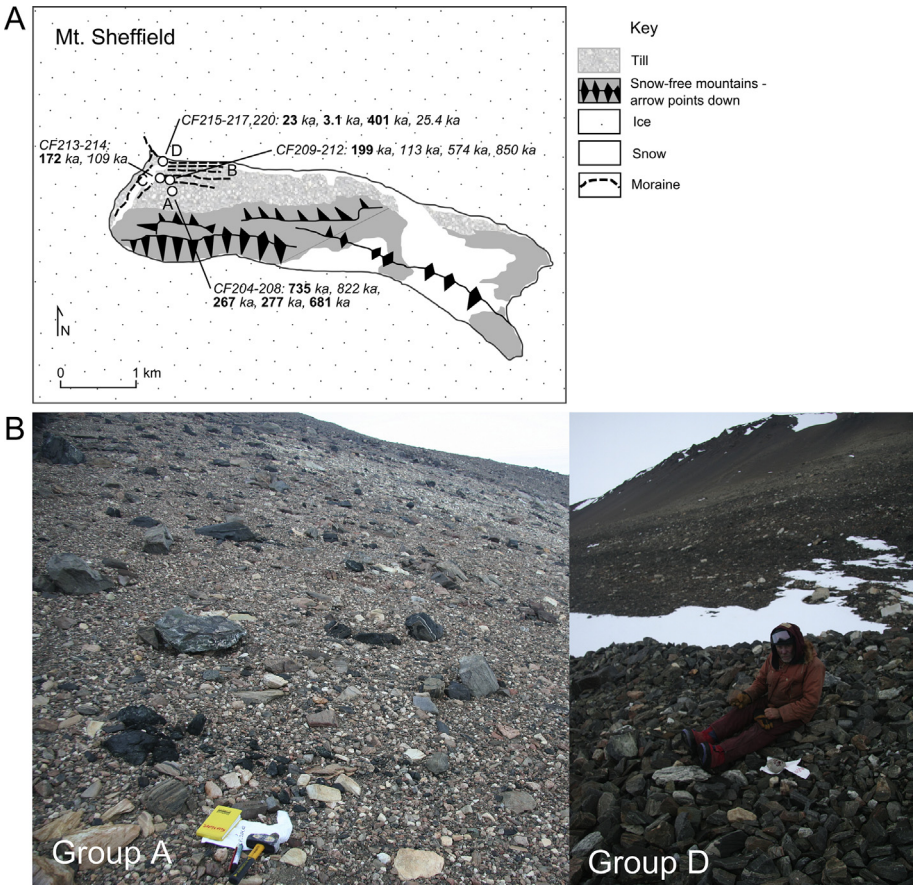


**Fig. 7.** A. Mt. Sheffield. The letters refer to the geomorphic groups discussed in the text. Sample location and ages are shown; those in bold have relatively simple exposure histories. B. Group A and D discussed in the text. A. Uppermost weathered pink till with few large clasts ($^{10}$Be age range: 267–822 ka). D. Coarse, angular/subangular till close to ice margin ($^{10}$Be age range: 3–401 ka).

stained than surrounding surfaces which suggests a local difference in erosion rate. Recent rock fracturing is one possibility which could partly explain the more complex exposure of this latter surface. Below the summit there is consistency in $^{26}$Al and $^{10}$Be concentrations between bedrock samples and a large perched boulder with minimum ages of around 600–800 ka. The one exception is a block (CF161) of local bedrock that probably reflects a local process. The deep weathering evident on these surfaces is consistent with continuous surface exposure and erosion as implied by the $^{26}$Al/$^{10}$Be ratios; if so, allowing for erosion since exposure, this suggests the bedrock ridge was exposed for most of the Pleistocene at elevations only 150–450 m above the adjacent Stratton Glacier.

This conclusion is supported by evidence for erosive-ice conditions on the lower mountain next to the modern margin of the tributary Stratton Glacier. Here all but one sample are young and have simple exposure histories. The data from ice-moulded bedrock indicate that erosive ice occupied this area before 41 ka and as late as 11.5 ka.

The results from the glacially eroded surface of Mt. Provender are consistent in demonstrating that a phase of erosion occurred prior to 800 ka (cf. Fogwill et al., 2004). Further, the summit does not appear to have been covered subsequently. Allowing for erosion of the weathered samples since exposure, the actual age of its exposure is likely to be much older.

### 4.2. Mt. Skidmore

The results from Mt. Skidmore come from erratics and the results are more complicated. However, the new data sheds light on the glacial history of Mt. Skidmore and reveals three important findings. First, Mt. Skidmore has not been over-ridden by eroding ice for millions of years. Second, there exists a trend of decreasing ice elevation through time. Third, Pleistocene ice thickening was cold-based and less than ~150 m.

#### 4.2.1. Upper bedrock surfaces (Group A)

The absence of erosive warm-based ice for millions of years is evident from bedrock on the weathered summit ridge (Group A) with an age of c. 1.5 Ma and an $^{26}$Al/$^{10}$Be ratio consistent with a relatively simple exposure history. This is a minimum age for the last deep erosion of this surface. This minimum age is supported by the great age of till in Group D from lower down the mountain where numerous clasts deposited on the weathered deposits have exposure ages of c. 1.5 Ma.

#### 4.2.2. Upper weathered till (Group D)

The ancient exposure ages for the pink till in Group D are consistent with the subdued morphology and weathering observed on these stable surfaces. Minimum exposure ages are consistently older than c. 700 ka. Samples with apparent simple exposure histories range in age between c. 700 ka and c. 1.5 Ma while the two oldest samples reveal a more complicated exposure history (Fig. 9).

Two simple scenarios can explain the observed age range and scatter in $^{26}$Al/$^{10}$Be ratios for this group. The first is periodic ice cover before c. 1.5 Ma with continuous surface exposure since. In this scenario the spread of exposure ages and $^{26}$Al/$^{10}$Be ratios reflect erosion from earlier than c. 1.5 Ma to c. 700 ka. This would imply

Please cite this article in press as: Hein, A.S., et al., Geological scatter of cosmogenic-nuclide exposure ages in the Shackleton Range, Antarctica: Implications for glacial history, Quaternary Geochronology (2013), http://dx.doi.org/10.1016/j.quageo.2013.03.008

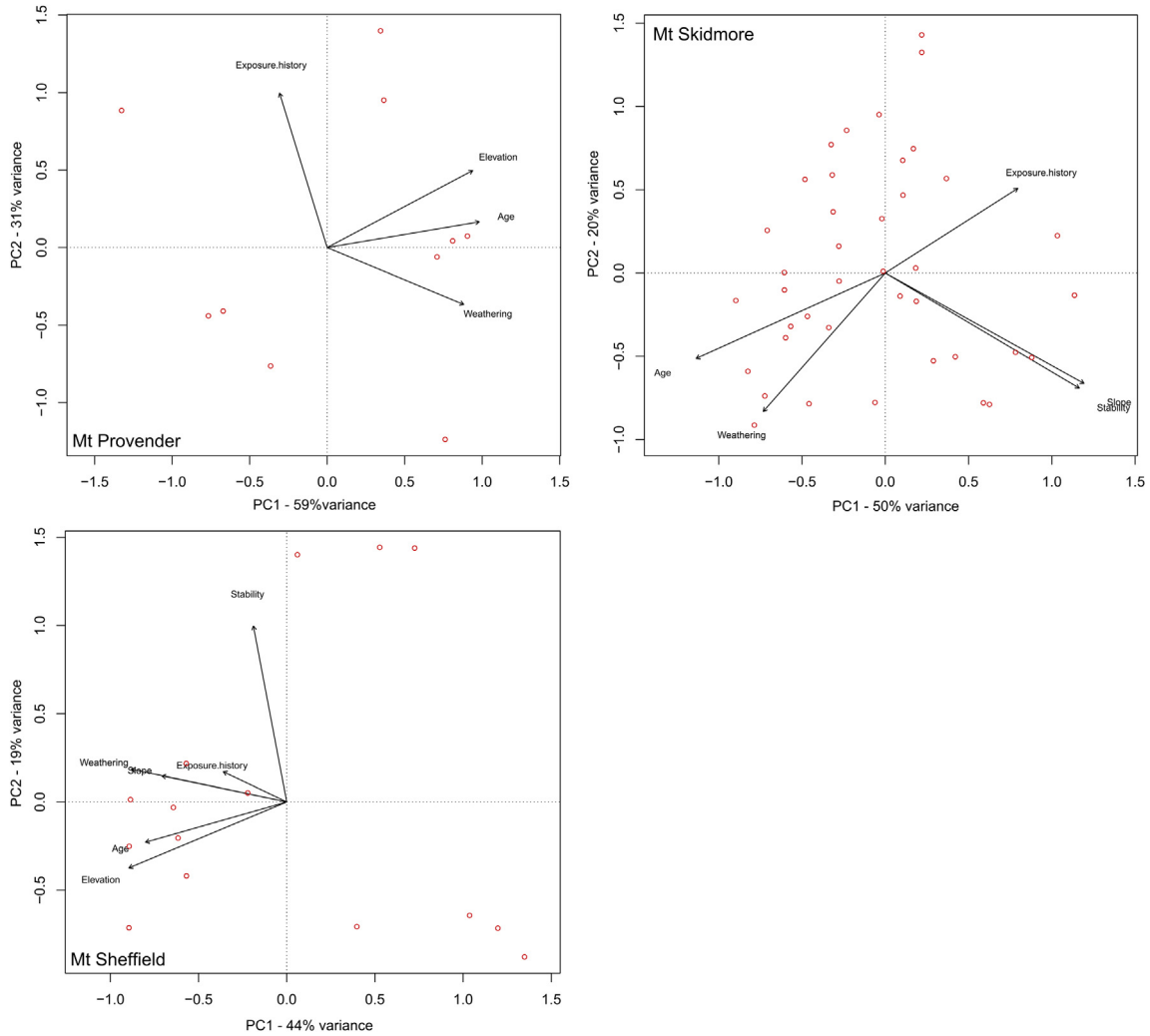


**Fig. 8.** The figure presents results of the Principal Component Analysis (PCA) for each site. The output of the PCA is a biplot displaying the samples (dots) and variables as labelled vectors scaled according to their eigenvalues. The percent of the total variance explained by each principal component is labelled on their individual axes. The first principal component is the *x*-axis and the second principal component is the *y*-axis. The length and direction of vectors relates to the rate of change and direction of most abundance (Kent and Coker, 1996). With reference to the scoring system in Table 1, the plot allows visualisation of the degree of correlation between variables. The most strongly correlated variables are those whose vectors are long and align together primarily along the principal *x*-axis (PC1) and secondarily along the *y*-axis (PC2). For example, age and weathering are strongly correlated at Mt. Skidmore where they align in the same quadrant and thus are correlated in both PC1 and PC2, whereas the exposure history is inversely correlated in both PC1 and PC2. A scatter plot comparing age and weathering would show a trend whereas this trend would not exist against exposure history. The PCA correlation matrix analysis was carried out using R (v.2.12.1) and the function pca.cor and using the data in Table DR1 as input.

that the younger samples with simple exposures were gradually exhumed through surface erosion, with perhaps subsequent disturbance on polygon margins (Morgan et al., 2011; Schafer et al., 1999). The more complex exposure histories would require erosion and rock fracturing, a process consistent with the angular nature of the till. After c. 700 ka, active erosion ceased and the surface has remained unmodified since; this is consistent with the high degree of weathering observed on all clasts. The second scenario involves short periods of burial by debris-rich cold-based ice earlier than c. 1.5 Ma and continuing until c. 700 ka. The range of exposure ages and ratios would reflect different amounts of erosion, inheritance or burial on or below the surface, and the addition of new material deposited by over-riding ice. Any burial period must have been short since several older clasts have apparent simple exposures.

It is not possible to differentiate the two with certainty but the exposure ages and geomorphology suggest that till on this part of Mt. Skidmore has had a long exposure history and one which implies no cover by erosive ice for millions of years. In addition, the surface has been mainly ice-free and unmodified for at least the past 700 ka. The exposure age probably indicates a minimum age for the end of active erosion at this site and/or an end to periodic burial by debris-rich cold-based ice.

These results contrast with those from Group C located further west at a similar elevation. Here the ages are remarkably consistent in the face of present surface slope activity and despite being taken from two locations and three lithologies. This less weathered till is much younger (c. 350 ka) than samples in Group D and there is a consistent complex exposure history. The simplest explanation is prolonged burial by local ice which did not deposit or move material. This could be explained by expansion of ice around the present ice-covered meltwater gully nearby or by the expansion of Ice Tongues A and B. The exposure ages suggests that ice expansion occurred at a time when the adjacent surface near Group D remained exposed (i.e., after 700 ka). The implication is that this burial signal reflects local conditions rather than overriding by the surrounding ice-sheet.

Please cite this article in press as: Hein, A.S., et al., Geological scatter of cosmogenic-nuclide exposure ages in the Shackleton Range, Antarctica: Implications for glacial history, Quaternary Geochronology (2013), http://dx.doi.org/10.1016/j.quageo.2013.03.008

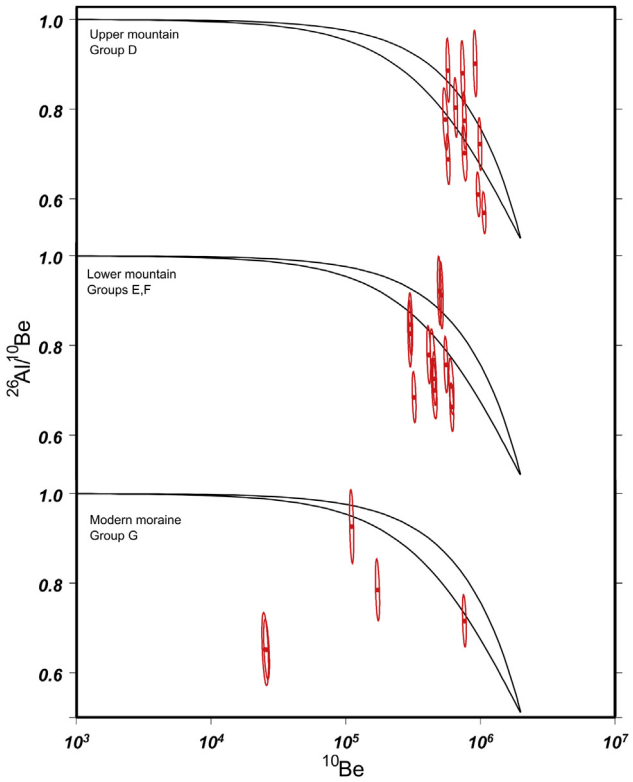


**Fig. 9.** Mt. Skidmore $^{26}$Al/$^{10}$Be ratio plots showing the difference in the $^{26}$Al/$^{10}$Be ratios between the upper mountain (upper plot) where exposures are oldest and most fall within the erosion island, the lower mountain (middle plot) where exposure ages are younger and most ratios fall into the complex zone below the erosion saturation line, and the modern moraine (lower plot) where a random mix of exposure ages and ratios occur.

#### 4.2.3. Lower slopes (Groups E and F)

Lower down the mountain below the weathering break first noted by Höfle and Buggisch (1995) at c. 400 m the till is comparatively less-weathered and is subject to more slope processes than on higher slopes. There is a corresponding shift in the cosmogenic nuclide data towards younger exposure ages and more complex exposure histories (Fig. 9). Minimum exposure ages are consistently older than c. 350 ka and with one exception, do not exceed 780 ka. Two samples give $^{26}$Al/$^{10}$Be ratios that fall on the line of apparent continuous surface exposure for c. 600 ka while the remainder are more complex.

The spread in ages partly results from rock fracture and exhumation. Several samples were angular and some young samples were taken from polygon margins where exhumation from beneath regolith is more likely. The shift of $^{26}$Al/$^{10}$Be ratios into the complex exposure zone could reflect either this churning within the regolith, rock fracturing or a burial signal. In this context, burial by water is a possibility. The presence of horizontal terraces indicates an elevated lake level in the past. Furthermore, the flattened surface free of upstanding boulders resembles surfaces moulded by floating ice (Hansom, 1983). Finally, any late Pleistocene thickening apparently did not result in deposition of new material.

#### 4.2.4. Modern moraine (Group G)

The cosmogenic nuclide results show a wide range of exposure ages covering a 1 million year period with both complicated and relatively continuous exposure histories (Fig. 9). This is typical of inheritance resulting from recycling and re-deposition of material. This is the only active depositional landform that was sampled, but given the amount of long-lived till in the region, the results are unsurprising. Nevertheless, the youngest ages do occur on the modern moraine. One sample with a relatively simple exposure history has an age of 120 ka, while the youngest sample which was measured twice has an age of 27 ka but with a burial history suggesting it does not date to the LGM as previously reported (Hein et al., 2011). These results are interesting given that such a random spread of ages is not found in till from Group F on the adjacent lower mountain where exposure ages are consistently older than 350 ka. The presence of sandstone clasts which were not found on the modern moraine suggest the latter till may have been deposited under different glaciological conditions than today. One possible explanation for the burial signal and lack of clasts younger than c. 350 ka is that late Pleistocene thickening simply resulted in raising the lake level without bringing in new material; this would also explain the elevated lake terraces.

#### 4.2.5. Overall Skidmore pattern

There is an ice surface lowering trend through time and an inference for an upper limit on mid – late Pleistocene ice thickening of less than 150 m. The conclusion is based on differences in the geomorphology, age and exposure history of clasts in the high elevation Group D, which have older, simpler exposures when compared to the younger and more complex exposure histories of the lower elevation Groups E – G (Fig. 9). The large spread in exposure ages and scatter in $^{26}$Al/$^{10}$Be ratios evident in these 30 samples may be influenced by inheritance and measurement uncertainty, but the overall consistency and clustering of the results within each group implies a non-random process above the modern moraine. This in turn suggests that the ratios mainly reflect the different exposure histories of the upper and lower surfaces.

There is evidence that ice thickened during the Pleistocene and covered slopes adjacent to Slessor Glacier and local tributaries, but that the magnitude of thickening and in some cases, extension, was limited. In addition to evidence of some form of burial from the lower mountain slopes, erratics from Group A indicate that the summit ridge was covered by cold-based ice during the Pleistocene, reflecting expansion of Stratton Glacier and Ice Tongue A. Here, erratics with complex exposure histories and ages of 420–600 ka are located up to 100 m above Ice Tongue A while the highest (150 m above ice) and oldest erratic at 880 ka has an apparent simple exposure representing an earlier advance. Expansion of Ice Tongue A and B or extensive burial by ice during the Pleistocene could explain the consistent young ages and burial signal evident in samples from Group C. Finally, an upper limit on the amount of thickening is provided by the data from Group D. The data suggest this area, between 575 m and 380 m elevation was ice free for most of the Pleistocene. These surfaces are just over 100 m above the adjacent Köppen Glacier.

### 4.3. Mt. Sheffield

Mt. Sheffield is situated on the margin of Slessor Glacier and the difference in ice dynamics is evident in the geomorphology and exposure age results. The surfaces have been shaped by moving ice and have not subsequently been modified by cryoturbation processes, and the young ages on the modern ice margin (Group D) indicate that inheritance is low. The upper slopes of Group A give the oldest set of exposure ages. Here, two pairs of near-identical exposure ages of 270 ka and c. 700 ka exist with simple exposure histories. There is no way of distinguishing the younger rock from the older rock in the field. They were taken in close proximity to each other, there is no evidence for major surface motion, and their degree of weathering does not match their age. Therefore it is difficult to infer recent exhumation to explain the young ages or recycling to explain the old ages. One possibility is that the till

Please cite this article in press as: Hein, A.S., et al., Geological scatter of cosmogenic-nuclide exposure ages in the Shackleton Range, Antarctica: Implications for glacial history, Quaternary Geochronology (2013), http://dx.doi.org/10.1016/j.quageo.2013.03.008

represents multiple advances. The older till is represented by the small, pink, angular till, which is draped by the larger darker clasts of the younger till (Fig. 7b). Lower down the mountain the exposure ages systematically decrease with the exception of a few outliers. The key finding at Mt. Sheffield is that there does appear to be a long-term ice-surface lowering trend since 700 ka.

## 5. Conclusions and wider implications

### 5.1. Exposure dating in Antarctica

This project produced one of the largest, most complicated multi-nuclide datasets in Antarctica. When apparently similarly weathered clasts on the same surface have vastly different exposure ages and histories, one begins to question whether fundamental ideas that guide field sampling apply in Antarctica. In this paper we have tried to unravel some of the reasons behind the scatter of ages.

The results of the PCA at all three sites demonstrate that the expected correlations do indeed exist within such 'noise'. To summarise: 1) the least-weathered and youngest-looking clasts give the youngest exposure ages, and vice versa; 2) the exposure ages increase with elevation above the modern ice; and 3) the oldest ages or most reliable ages are found on flat stable surfaces. The results are reassuring for those interested in dating ice-sheet change using cosmogenic nuclide altitude-profiles.

The PCA analyses at Mt. Skidmore also highlighted an interesting correlation in that clasts with young exposure ages have more complex exposure histories. The cause in the context of Mt. Skidmore is related to recent exhumation, rock-fracturing or periodic burial by ice. Such a correlation may be common in areas covered from time to time by cold-based ice where there is opportunity for clasts to have longer and more complicated exposure histories. In Antarctica this is likely to be the norm on the flanks of outlet glaciers and around the margins of local glaciers because any fluctuations in ice thickness usually involves cold-based ice. One interesting finding is of a clast reported with an apparent $^{10}$Be LGM exposure age of 27 ka (Hein et al., 2011) which had in fact been buried for a long period and the exposure signal had been inherited from earlier times.

Finally, the study highlights the need for nuclide pairings capable of detecting short periods of burial under ice, which is a limitation of the $^{26}$Al/$^{10}$Be ratio. Recent research has aimed to improve extraction techniques, nuclide systematics and measurements of in situ produced $^{14}$C, an isotope with a short half-life which will make it possible to detect even short periods of burial by ice (Hippe et al., 2009; Lifton et al., 2001; Naysmith et al., 2004; Pigati and Lifton, 2004; Yokoyama et al., 2004). The $^{14}$C/$^{10}$Be pairing would be ideal for investigating late Pleistocene ice thickness changes in Antarctica (White et al., 2011).

### 5.2. Glacial history

The cosmogenic-nuclide ages of bedrock and glacial erratics on three sites on the northern flanks of the Shackleton Range gives several insights into the longer-term history of Slessor Glacier.

The great age of high-elevation surfaces in the Shackleton Range that have been moulded by overriding ice is demonstrated by exposure ages of more than c. 800 ka. If one allows for the loss of nuclides through surface erosion, then such ages are a minimum and the true ages will be in millions of years. It seems likely that these upper weathered surfaces shaped by overriding warm-based ice are similar to those elsewhere in the Transantarctic Mountains and date back at least to the Miocene ~14 Ma, before the development of the cold polar climate of today (Denton and Sugden, 2005). Indeed, the step change from a Greenland-type climate with meltwater issuing from mountain glaciers in the mountains has been pinned down by argon–argon dating of volcanic ashes in the Dry Valleys to ~14 Ma (Lewis et al., 2008).

The discovery that the oldest samples on both Mt. Skidmore and Mt. Provender may have simple exposure histories suggests that the higher flanks of these mountains may have been free of ice for ~800 ka. Although the technique is not able to rule out short-lived coverage by ice, there is no evidence to indicate significant ice coverage for at least the later Pleistocene.

All three locations reveal an overall pattern of ice elevations that have lowered progressively over time. Thus in general the oldest samples tend to occur at high elevations while there are a greater proportion of younger samples at lower elevations. However, there is a great deal of noise and we have tried to highlight some of the processes that can lead to a scatter in the data. The pattern of progressive lowering would be expected in that long-term glacial erosion by bounding outlet glaciers and associated isostatic rise of adjacent mountains in response would lower the ice surface in relation to the mountains (e.g., Bromley et al., 2010; Stern et al., 2005).

The elevation of a change from old exposure ages with simple exposure above to a range of younger ages with complex exposure below can be interpreted in one of two ways. First, the magnitude of adjacent ice thickening during the mid to late Pleistocene compared to the present is less than ~150 m. It is the history of repeated inundation by thickening cold-based ice that causes a mix of younger clasts with complex exposures. This conclusion, if it also applied to outlet glaciers elsewhere in Antarctica, would be an important constraint on maximum volume changes of the Antarctic ice sheet during the Pleistocene. Second, the difference may be due to a difference in weathering between the upper and lower slopes.

The $^{10}$Be exposure ages on clasts on moraines on the flanks of Slessor Glacier 80 km above its grounding line cluster in two intervals in the Pleistocene, namely 270 ka and 700 ka. Taken at face value this implies that the glacier, an outlet glacier of the East Antarctic Ice Sheet either thickened by c. 150 m in these two intervals, or that it has lowered its surface the same amount by eroding the bed subsequently.

## 6. Conclusion

The cosmogenic-nuclide results from the Shackleton Range highlight the extreme complexity and challenge of exposure dating in polar environments. Interpretation of such data is strongly dependent on geomorphological observations. Increasing the density of measurements gives a statistical advantage which can greatly improve such interpretations. In areas subjected to erosive warm-based ice cover, increasing the density of single nuclide measurements may suffice. However in areas inundated by cold-based ice, a multi-nuclide approach is necessary to better understand the long-term glacial history.

## Acknowledgements

We thank the UK Natural Environment Research Council (NERC) and the Scottish Alliance for Geoscience, Environment and Society (SAGES); Antarctic Logistics and Expeditions (ALE) for Fogwill's field support; Bronwen Whitney for help generating the PCA plots; I. Joughin for supplying ice-velocity data; A. Le Brocq for bathymetry; and E. McDougall for laboratory support. We thank Patrick Applegate and an anonymous reviewer for their constructive comments.

*Editorial handling by*: S. Ivy-Ochs

## Appendix A. Supplementary data

Supplementary data related to this article can be found at http://dx.doi.org/10.1016/j.quageo.2013.03.008.

## References

Ackert Jr., R.P., Mukhopadhyay, S., Pollard, D., DeConto, R.M., Putnam, A.E., Borns Jr., H.W., 2011. West Antarctic Ice Sheet elevations in the Ohio Range: geologic constraints and ice sheet modeling prior to the last highstand. Earth And Planetary Science Letters 307, 83–93.

Ackert, R.P., Mukhopadhyay, S., Parizek, B.R., Borns, H.W., 2007. Ice elevation near the West Antarctic Ice Sheet divide during the Last Glaciation. Geophysical Research Letters 34.

Applegate, P.J., Urban, N.M., Keller, K., Lowell, T.V., Laabs, B.J.C., Kelly, M.A., Alley, R.B., 2012. Improved moraine age interpretations through explicit matching of geomorphic process models to cosmogenic nuclide measurements from single landforms. Quaternary Research 77, 293–304.

Balco, G., 2011. Contributions and unrealized potential contributions of cosmogenic-nuclide exposure dating to glacier chronology, 1990–2010. Quaternary Science Reviews 30, 3–27.

Balco, G., Stone, J.O., Lifton, N.A., Dunai, T.J., 2008. A complete and easily accessible means of calculating surface exposure ages or erosion rates from Be-10 and Al-26 measurements. Quaternary Geochronology 3, 174–195.

Bentley, M.J., Fogwill, C.J., Le Brocq, A.M., Hubbard, A.L., Sugden, D.E., Dunai, T.J., Freeman, S., 2010. Deglacial history of the West Antarctic Ice Sheet in the Weddell Sea embayment: Constraints on past ice volume change. Geology 38, 411–414.

Briner, J.P., Gosse, J.C., Bierman, P.R., 2006. Applications of cosmogenic nuclides to Laurentide Ice Sheet history and dynamics. Special Paper 415. In: Situ-Produced Cosmogenic Nuclides and Quantification of Geological Processes, vol. 415, pp. 29–41.

Bromley, G.R.M., Hall, B.L., Stone, J.O., Conway, H., Todd, C.E., 2010. Late Cenozoic deposits at Reedy Glacier, Transantarctic mountains: implications for former thickness of the West Antarctic Ice Sheet. Quaternary Science Reviews 29, 384–398.

Brommer, A., Millar, I.L., Zeh, A., 1999. Geochronology, structural geology and petrology of the northwestern La Grange Nunataks, Shackleton Range, Antarctica. Terra Antarctica 6, 269–278.

Chmeleff, J., von Blanckenburg, F., Kossert, K., Jakob, D., 2010. Determination of the Be-10 half-life by multicollector ICP-MS and liquid scintillation counting. Nuclear Instruments & Methods in Physics Research Section B-Beam Interactions with Materials and Atoms 268, 192–199.

Denton, G.H., Sugden, D.E., 2005. Meltwater features that suggest Miocene ice-sheet overriding of the Transantarctic Mountains in Victoria Land, Antarctica. Geografiska Annaler Series A-Physical Geography 87A, 67–85.

Desilets, D., Zreda, M., Prabu, T., 2006. Extended scaling factors for in situ cosmogenic nuclides: new measurements at low latitude. Earth and Planetary Science Letters 246, 265–276.

Dunai, T.J., 2001. Influence of secular variation of the geomagnetic field on production rates of in situ produced cosmogenic nuclides. Earth and Planetary Science Letters 193, 197–212.

Fogwill, C.J., Bentley, M.J., Sugden, D.E., Kerr, A.R., Kubik, P.W., 2004. Cosmogenic nuclides Be-10 and Al-26 imply limited Antarctic Ice Sheet thickening and low erosion in the Shackleton Range for >1 m y. Geology 32, 265–268.

Fogwill, C.J., Hein, A.S., Bentley, M.J., Sugden, D.E., 2012. Do blue-ice moraines in the Heritage Range show the West Antarctic ice sheet survived the last interglacial? Palaeogeography, Palaeoclimatology, Palaeoecology 335, 61–70.

Gosse, J.C., Phillips, F.M., 2001. Terrestrial in situ cosmogenic nuclides: theory and application. Quaternary Science Reviews 20, 1475–1560.

Hallet, B., Putkonen, J., 1994. Surface dating of dynamic landforms – young boulders on aging moraines. Science 265, 937–940.

Hansom, J.D., 1983. Shore-platform development in the South Shetland Islands, Antarctica. Marine Geology 53, 211–229.

Haran, T., Bohlander, J., Scambos, T., Painter, T., Fahnestock, M., 2005. MODIS Mosaic of Antarctica (MOA) Image Map. National Snow and Ice Data Center. Digital Media, Boulder, Colorado USA. updated 2006.

Hein, A.S., Fogwill, C.J., Sugden, D.E., Xu, S., 2011. Glacial/interglacial ice-stream stability in the Weddell Sea embayment, Antarctica. Earth And Planetary Science Letters 307, 211–221.

Hippe, K., Kober, F., Baur, H., Ruff, M., Wacker, L., Wieler, R., 2009. The current performance of the in situ (14)C extraction line at ETH. Quaternary Geochronology 4, 493–500.

Höfle, H.-C., Buggisch, W., 1995. Glacial geology and Petrography of erratics in the Shackleton Range, Antarctica. Polarforschung 63, 183–201.

Ivins, E.R., James, T.S., 2005. Antarctic glacial isostatic adjustment: a new assessment. Antarctic Science 17, 541–553.

Jezek, K., Team, R.P., 2002. RAMP AMM-1 SAR Image Mosaic of Antarctica. Alaska SAR Facility, Fairbanks, AK (in association with the National Snow and Ice Data Center, Boulder, CO. Digital media).

Jolliffe, I.P., 2002. Principal Component Analysis, second ed. Springer, New York.

Joughin, I., Bamber, J.L., 2005. Thickening of the Ice Stream Catchments Feeding the Filchner-Ronne Ice Shelf, Antarctica, 6, pp. 353–360.

Kent, M., Coker, P., 1996. Vegetation Description and Analysis, A Practical Approach. John Wiley and Sons, London.

Kerr, A., Hermichen, W.D., 1999. Glacial modification of the Shackleton Range, Antarctica. Terra Antarctica 6, 353–360.

Korschinek, G., Bergmaier, A., Faestermann, T., Gerstmann, U.C., Knie, K., Rugel, G., Wallner, A., Dillmann, I., Dollinger, G., von Gostomski, C.L., Kossert, K., Maiti, M., Poutivtsev, M., Remmert, A., 2010. A new value for the half-life of Be-10 by Heavy-Ion Elastic Recoil Detection and liquid scintillation counting. Nuclear Instruments & Methods in Physics Research Section B-Beam Interactions with Materials and Atoms 268, 187–191.

Lal, D., 1991. Cosmic-ray labeling of erosion surfaces – Insitu nuclide production-rates and erosion models. Earth And Planetary Science Letters 104, 424–439.

Lewis, A.R., Marchant, D.R., Ashworth, A.C., Hedenas, L., Hemming, S.R., Johnson, J.V., Leng, M.J., Machlus, M.L., Newton, A.E., Raine, J.I., Willenbring, J.K., Williams, M., Wolfe, A.P., 2008. Mid-Miocene cooling and the extinction of tundra in continental Antarctica. Proceedings of the National Academy of Sciences of the United States of America 105, 10676–10680.

Lifton, N.A., Bieber, J.W., Clem, J.M., Duldig, M.L., Evenson, P., Humble, J.E., Pyle, R., 2005. Addressing solar modulation and long-term uncertainties in scaling secondary cosmic rays for in situ cosmogenic nuclide applications. Earth and Planetary Science Letters 239, 140–161.

Lifton, N.A., Jull, A.J.T., Quade, J., 2001. A new extraction technique and production rate estimate for in situ cosmogenic C-14 in quartz. Geochimica Et Cosmochimica Acta 65, 1953–1969.

Liu, H., Jezek, K., Li, B., Zhao, Z., 2001. Radarsat Antarctic Mapping Project Digital Elevation Model Version 2. National Snow and Ice Data Center. Digital Media, Boulder, CO.

Mackintosh, A., White, D., Fink, D., Gore, D.B., Pickard, J., Fanning, P.C., 2007. Exposure ages from mountain dipsticks in Mac. Robertson Land, East Antarctica, indicate little change in ice-sheet thickness since the Last Glacial Maximum. Geology 35, 551–554.

Margerison, H.R., Phillips, W.M., Stuart, F.M., Sugden, D.E., 2005. Cosmogenic He-3 concentrations in ancient flood deposits from the Coombs Hills, northern Dry Valleys, East Antarctica: interpreting exposure ages and erosion rates. Earth And Planetary Science Letters 230, 163–175.

Morgan, D.J., Putkonen, J., Balco, G., Stone, J., 2011. Degradation of glacial deposits quantified with cosmogenic nuclides, Quartermain Mountains, Antarctica. Earth Surface Processes And Landforms 36, 217–228.

Naysmith, P., Cook, G.T., Phillips, W.M., Lifton, N.A., Anderson, R., 2004. Preliminary results for the extraction and measurement of cosmogenic in situ C-14 from quartz. Radiocarbon 46, 201–206.

Nishiizumi, K., 2004. Preparation of Al-26 AMS standards. Nuclear Instruments & Methods in Physics Research Section B 223–24, 388–392.

Nishiizumi, K., Winterer, E.L., Kohl, C.P., Klein, J., Middleton, R., Lal, D., Arnold, J.R., 1989. Cosmic-ray production-rates of Be-10 and Al-26 in quartz from glacially Polished Rocks. Journal of Geophysical Research-Solid Earth and Planets 94, 17907–17915.

Nishiizumi, K., Imamura, M., Caffee, M.W., Southon, J.R., Finkel, R.C., McAninch, J., 2007. Absolute calibration of Be-10 AMS standards. Nuclear Instruments & Methods in Physics Research Section B. 258, 403–413.

Pigati, J.S., Lifton, N.A., 2004. Geomagnetic effects on time-integrated cosmogenic nuclide production with emphasis on in situ C-14 and Be-10. Earth and Planetary Science Letters 226, 193–205.

Porter, S.C., Swanson, T.W., 2008. Cl-36 dating of the classic Pleistocene glacial record in the northeastern Cascade Range, Washington. American Journal of Science 308, 130–166.

Schafer, J.M., Ivy-Ochs, S., Wieler, R., Leya, J., Baur, H., Denton, G.H., Schluchter, C., 1999. Cosmogenic noble gas studies in the oldest landscape on earth: surface exposure ages of the Dry Valleys, Antarctica. Earth And Planetary Science Letters 167, 215–226.

Skidmore, M.J., Clarkson, P.D., 1972. Physiography and glacial geomorphology of the Shackleton Range. British Antarctic Survey Bulletin 30, 69–80.

Stern, T.A., Baxter, A.K., Barrett, P.J., 2005. Isostatic rebound due to glacial erosion within the Transantarctic Mountains. Geology 33, 221–224.

Stone, J.O., 2000. Air pressure and cosmogenic isotope production. Journal of Geophysical Research-Solid Earth 105, 23753–23759.

Stone, J.O., Balco, G.A., Sugden, D.E., Caffee, M.W., Sass, L.C., Cowdery, S.G., Siddoway, C., 2003. Holocene deglaciation of Marie Byrd Land, West Antarctica. Science 299, 99–102.

Storey, B.C., Fink, D., Hood, D., Joy, K., Shulmeister, J., Riger-Kusk, M., Stevens, M.I., 2010. Cosmogenic nuclide exposure age constraints on the glacial history of the Lake Wellman area, Darwin Mountains, Antarctica. Antarctic Science 22, 603–618.

Sugden, D.E., Balco, G., Cowdery, S.G., Stone, J.O., Sass, L.C., 2005. Selective glacial erosion and weathering zones in the coastal mountains of Marie Byrd Land, Antarctica. Geomorphology 67, 317–334.

Swanger, K.M., Marchant, D.R., Schaefer, J.M., Winckler, G., Head Iii, J.W., 2011. Elevated East Antarctic outlet glaciers during warmer-than-present climates in southern Victoria Land. Global And Planetary Change 79, 61–72.

Todd, C., Stone, J., Conway, H., Hall, B., Bromley, G., 2010. Late Quaternary evolution of Reedy Glacier, Antarctica. Quaternary Science Reviews 29, 1328–1341.

White, D., Fueloep, R.-H., Bishop, P., Mackintosh, A., Cook, G., 2011. Can in-situ cosmogenic (14)C be used to assess the influence of clast recycling on exposure dating of ice retreat in Antarctica? Quaternary Geochronology 6, 289–294.

Whitehouse, P.L., Bentley, M.J., LeBrocq, A.M., 2012. A deglacial model for Antarctica: geological constraints and glaciological modelling as a basis for a new model of glacial isostatic adjustment. Quaternary Science Reviews 32, 1–24.

Yokoyama, Y., Caffee, M.W., Southon, J.R., Nishiizumi, K., 2004. Measurements of in situ produced C-14 in terrestrial rocks. Nuclear Instruments & Methods in Physics Research Section B-Beam Interactions with Materials and Atoms 223, 253–258.

Please cite this article in press as: Hein, A.S., et al., Geological scatter of cosmogenic-nuclide exposure ages in the Shackleton Range, Antarctica: Implications for glacial history, Quaternary Geochronology (2013), http://dx.doi.org/10.1016/j.quageo.2013.03.008